Design of Chimeric Histone Deacetylase- and Tyrosine Kinase-Inhibitors: A Series of Imatinib Hybrides as Potent Inhibitors of Wild-Type and Mutant BCR-ABL, PDGF-Rβ, and Histone Deacetylases†

Siavosh Mahboobi,*,‡ Stefan Dove,‡ Andreas Sellmer,‡ Matthias Winkler,‡ Emerich Eichhorn,‡ Herwig Pongratz,‡ Thomas Ciossek,§,▽ Thomas Baer,§,△ Thomas Maier,§ and Thomas Beckers*,||

Institute of Pharmacy, University of Regensburg, D-93040 Regensburg, Germany, and Nycomed GmbH, Therapeutic Area Oncology, Byk-Gulden Strasse 2, D-78467 Konstanz, Germany

Received August 5, 2008

Inhibitors of histone deacetylases are a new class of cancer therapeutics with possibly broad applicability. Combinations of HDAC inhibitors with the kinase inhibitor **1** (Imatinib) in recent studies showed additive and synergistic effects. Here we present a new concept by combining inhibition of protein kinases and HDACs, two independent pharmacological activities, in one synthetic small molecule. In general, the HDAC inhibition profile, the potencies, and the probable binding modes to HDAC1 and HDAC6 were similar as for **6** (SAHA). Inhibition of Abl kinase in biochemical assays was maintained for most compounds, but in general the kinase selectivity profile differed from that of **1** with nearly equipotent inhibition of the wild-type and the Imatinib resistant Abl $T^{315}I$ mutant. A potent cellular inhibition of PDGFR and cytotoxicity toward EOL-1 cells, a model for idiopathic hypereosinophilic syndrome (HES), are restored or enhanced for selected analogues (**12b**, **14b**, and **18b)**. Cytotoxicity was evaluated by using a broad panel of tumor cell lines, with selected analogues displaying mean IC_{50} values between 3.6 and 7.1 μM.

Introduction

Selective inhibition of protein kinases is an important therapeutic approach for the treatment of human cancers.[1] However, as extensively documented for the Bcr-Abl oncogene in chronic myeloid leukemia (CML)[a] patients treated with **1** (Imatinib, Figure 1A), clinical resistance caused by multiple mutations affecting **1** binding to the Bcr-Abl kinase protein has been observed.[2,3] One frequent mutation found is $T^{315}I$ within the ATP-binding site of Bcr-Abl, abrogating a direct hydrogen bond of **1** with T^{315} of Bcr-Abl.[2,4,5] In vitro studies of resistance to **1** indicate additional mechanisms, including overexpression of Bcr-Abl caused by gene amplification[6−8] and increased efflux mediated by the multidrug resistance P-glycoprotein (ABCB1, Pgp).[9] One strategy to circumvent drug resistance of CML patients to therapy with **1** is exemplified by recently approved drugs: the abl/src dual kinase inhibitor *N*-(2-chloro-6-methylphenyl)-2-(6-(4-(2-hydroxyethyl)piperazin-1-yl)-2-ethylpyrimidin-4-ylamino)thiazole-5-carboxamide, known as **2** (Dasatinib),[10,4] and the **1** analogue benzamide **3** (Nilotinib).[11,12] Whereas **3** is a more potent, close analogue of **1**also binding to the inactive abl kinase, **2** as a 2-aminopyridinyl-thiazole analogue inhibits abl and src kinases in the active as well as in the inactive conformation with high potency. Both agents are effective toward most clinically relevant Bcr-Abl mutants with the exception of the $T^{315}I$ mutant.[11,4]

A still preclinical strategy was exemplified by combination of **1** or **2** with inhibitors of histone deacetylases (HDIs). Cotreatment with **4** (LAQ 824),[13] a close analogue of **5** (LBH589),[14] or **6** (SAHA) as inhibitors of histone deacetylases increased the potency of **1** and **2**, inducing apoptosis of K562 and LAMA-84 blast crisis CML cell lines.[15,16] The combination showed additive or synergistic effects, which were explained by down-regulation of wild-type and mutant Bcr-Abl $T^{315}I$ protein.[13]

4, **5**, and **6** are broad spectrum inhibitors of HDAC class I and II enzymes.[17,18] Mammalian HDAC class I (isoenzymes 1−3, 8), class II (isoenzymes 4−7, 9, 10), and class IV (HDAC 11) isoenzymes are functionally related, Zn^{2+}-containing amidohydrolases inhibited by the natural compound **7** (Trichostatin A, or TSA).[19] HDAC enzymes catalyze the reversible deacetylation of acetylated lysine residues in respective substrates such as core histone proteins H2A/B, H3, and H4.[20] HDAC inhibitors, by inducing histone hyperacetylation, cause a relaxation of chromatin, correlating with a release from transcriptional repression.[20] Nevertheless, targets different from core histone proteins exist. This might explain the complex transcriptional signatures with up- and down-regulated genes seen in HDI treated cancer cells.[21,22] HDIs belonging to four different chemical classes are currently in phase I to III clinical development. **6** was approved for treatment of therapy resistant cutaneous T-cell lymphoma (CTCL).[23] **5**, **6**, and **8** (MS-275),[24]

† This paper is dedicated to Professor Gottfried Märkl on the occasion of his 80th birthday.

* Corresponding authors: S.M.: e-mail, siavosh.mahboobi@chemie.uni-regensburg.de; telephone, (+49) (0) 941-9434824; fax, (+49) (0) 941-9431737 (medicinal chemistry). T.B.: e-mail, Thomas.Beckers@oncotest.de; telephone, (+49) (0) 761-5155916; fax, (+49) (0) 761 51559 55 (pharmacology).

‡ University of Regensburg.

§ Nycomed GmbH.

▽ Present address: Boehringer Ingelheim Pharma, Germany.

△ Present address: Dottikon AG, Switzerland.

|| Present address: Oncotest GmbH, Institute for Experimental Oncology, Am Flughafen 12-14, D-79108 Freiburg, Germany.

[a] Abbreviations: APL, acute promyelocytic leukemia; AML, acute myelogenous leukemia; AMC, 7-amino-4-methylcoumarin; ATCC, American tissue type collection; BOP, 1-benzotriazolyloxy-tris-(dimethylamino)-phosphoniumhexafluorophosphate; CML, chronic myeloid leukemia; HDI, histone deacetylase inhibitor; HDAC, histone deacetylase; HDLP, histone deactetylase-like protein; HDAH, histone deacetylase-like amidohydrolase; HES, idiopathic hypereosinophilic syndrome; NSCLC, non small cell lung cancer; PDGFR, platelet derived growth factor receptor; PKA, protein kinase A; rHDAC, recombinant HDAC; SAHA, suberoylanilide hydroxamic acid; SDS, sodium dodecylsulfate; SDS-PAGE, SDS polyacrylamide gel electrophoresis; TSA, trichostatin A; VEGFR, vascular endothelial growth factor receptor.

10.1021/jm800988r CCC: $40.75
Published on Web 03/20/2009

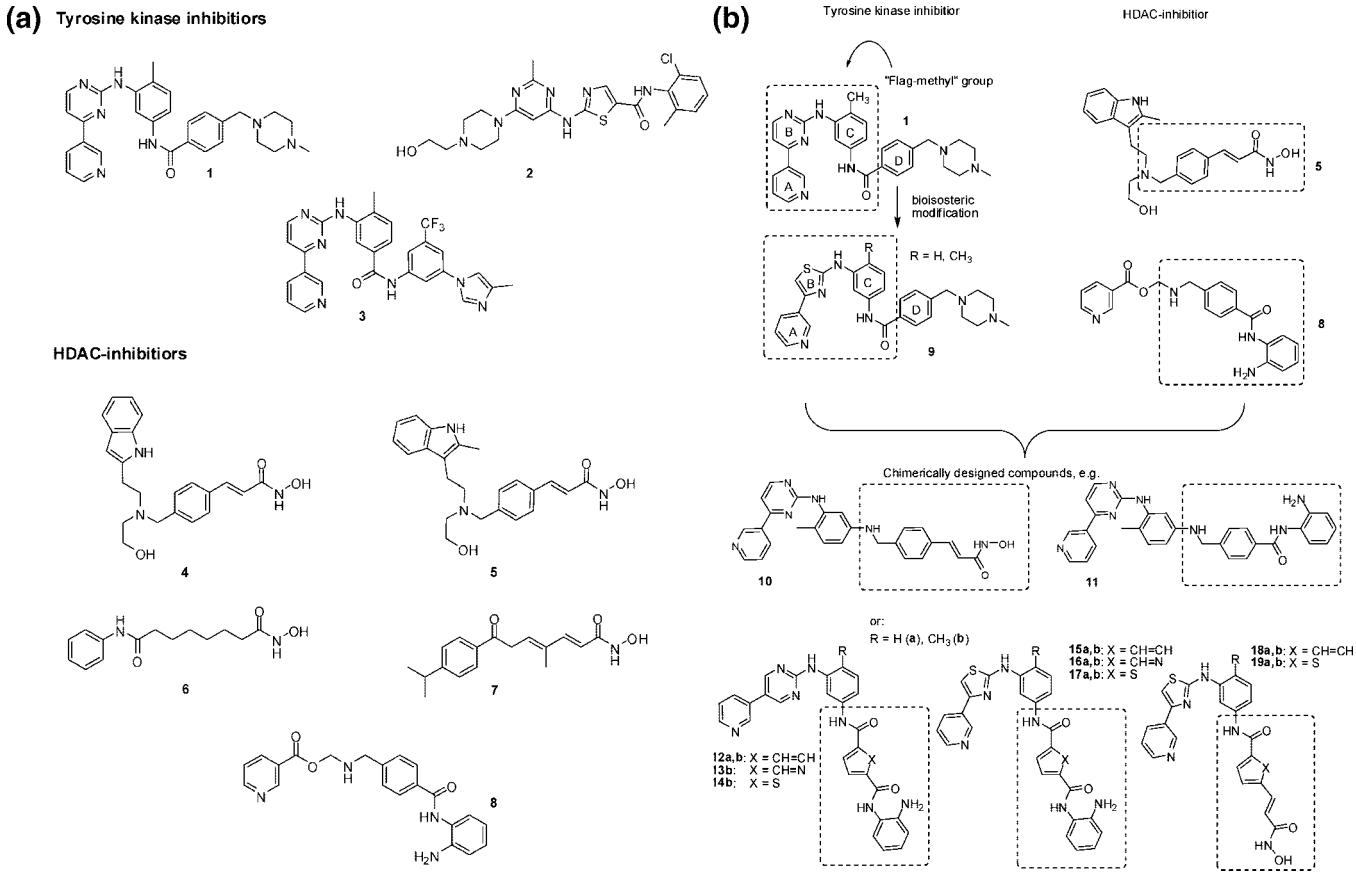

Figure 1. (A) Structures of Bcr-abl kinase inhibitors **1**, **2**, and **3** approved for treatment of CML, of HDAC inhibitors as the benzamide **8**, and of the hydroxamate class of compounds (**4**−**7**). (B) Concept of chimerically designed Imatinib-HDAC inhibitor hybrids by combining selected structural features of a tyrosine kinase- and a HDAC-inhibitor exemplified by chimeric structures **10**−**19b**.

examples for the prominent second generation HDAC inhibitors exhibiting the hydroxamic acid and benzamide Zn^{2+}-complexing motif (headgroup), are shown in Figure 1a.

Here we report on a novel tumor targeting strategy, combining the structural features of the Abl, PDGFRβ, and Kit inhibitor **1**, with respect to its bioisosteric thiazolyl derivative **9** (Figure 1b, exchange of the B-ring pyrimidine for a thiazole) with HDAC inhibitory head groups to overcome resistance to **1** by synergistic inhibition of two pharmacological targets. We selected the hydroxamic acid and benzamide motif, respectively, for combination with the *N*-(3-(4-(pyridin-3-yl)pyrimidin-2-ylamino)phenyl)amide core structure of **1**, or the *N*-(3-(4-(pyridin-3-yl)thiazol-2-ylamino)phenyl)amide of its bioisosteric analogue to obtain chimerically designed compounds. In early reports the so-called "Flag-methyl"-group[25,26] in the C-ring system (Figure 1b) has been described to be responsible for selectivity and enhancement of activity of the *N*-(3-(4-(pyridin-3-yl)thiazol-2-ylamino)phenyl)amide pharmacophore[25,26] concerning Bcr-Abl and PDGFR activity. Therefore, the effect of this substitution pattern has also been investigated.

Chemistry

The synthetic route to obtain the desired target compounds (Scheme 1) is given in the following: Catalytic reduction with hydrogen of the respective *N*-(3-nitrophenyl)-4-pyrimidin-2-amines **20a** and **20b** (Scheme 1), prepared as described,[25,27] led to the corresponding primary arylamines **21a**, **21b**, which were used as central intermediates. Reductive amination with (*E*)-3-(4-formylphenyl)acrylic acid (**22**) or methyl 4-formylbenzoate (**23**) led to the phenylacrylic acid **24** or to the methyl ester **25**, respectively; alkaline cleavage afforded the corresponding carboxylic acid **26**. Amidation of **24** with *O*-(tetrahydro-2*H*-pyran-2-yl)hydroxylamine (NH_2OTHP) (**27**), or rather of **26** with *tert*-butyl 2-aminophenylcarbamate (**28**),[28] mediated by BOP (1-benzotriazolyloxy-tris-(dimethylamino)phosphoniumhexafluorophosphate) as a coupling reagent,[29] led to **29** and **30**. After deprotection, the desired *N*-hydroxycinnamamide **10** and the *N*-(2-aminoaryl)benzamide **11** were obtained. The terephthalamide **31** was obtained by monomethylation of the amino intermediate **21a**, affording **32**, which was amidated with 4-(2-(*tert*-butoxycarbonylamino)phenylcarbamoyl)benzoic acid (**33**). The resulting *tert*-butyl-2-benzamidocarbamate **34** was deprotected with trifluoroacetic acid.

A closely related synthetic strategy (Scheme 2) was employed for the syntheses of several compounds of the hydroxamate and benzamide groups, exhibiting structural modifications also in the B- and D-ring systems (Figure 1b). The *N*-(3-nitrophenyl)thiazol-2-amines **35a** and **35b**, by catalytic reduction with hydrogen, yielded the arylamines **36a**, **36b**. These intermediates were used for amidation with the suitably protected and substituted carboxylic acids **37**−**42**. Amidation hereby was performed either by transformation of the corresponding carboxylic acids **37**−**39** and **42** to their carboxylic acid chlorides in a mixture of pyridine/thionyl chloride, followed by addition of the primary arylamino compounds **21a**, **21b** and **36a**, **36b**, respectively, or mediated by BOP.[29] Deprotection of the *tert*-butyl-2-benzamidocarbamates **43a**−**48b** with trifluoroacetic acid, respectively, of the *N*-(tetrahydro-2*H*-pyran-2-yloxy)cinnamamides **49a**−**50b** or *N*-(tetrahydro-2*H*-pyran-2-yloxy)benzamides **53a**, **53b** with hydrochloric acid led to the desired *N*-(2-

Scheme 1. Synthesis of Target Compounds **10**, **11**, and **31**[a]

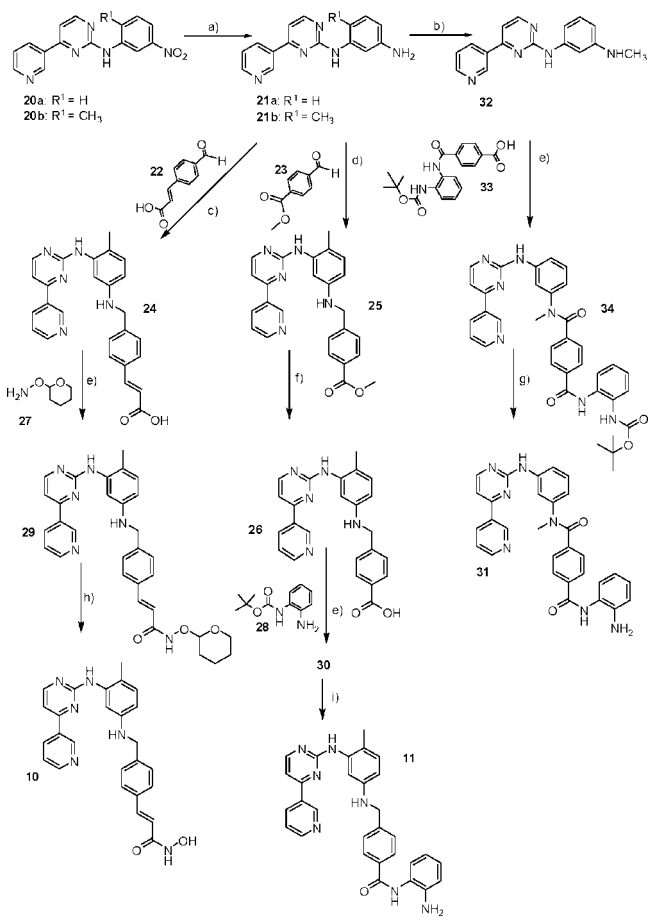

[a] Conditions: (a) H_2, Pd/C, 30 atm, 16 h; (b) paraformaldehyde, MeOH, NaOMe, Δ, then $NaBH_4$, Δ; (c) MeOH, HOAc, $NaBH_3CN$, 20° C, 14 h; (d) THF, HOAc, $NaBH(OAc)_3$, 40° C, 16 h; (e) THF, NEt_3, BOP, 20° C, 16 h or DMF, NEt_3, EDC·HCl; (f) MeOH, H_2O, LiOH, 20° C, 16 h; (g) dioxane, HCl, 20° C, 4 h; (h) MeOH, H_2O, HCl, 20° C, 16 h; (i) CF_3COOH, 20° C, 1 h.

arylamino)arylcarboxamides **12a**−**17b** and *N*-hydroxacrylamides **18a**−**19b**, respectively, to the hydroxamic acids **54a**−**54b**.

The *N*-(3-nitrophenyl)thiazol-2-amines **35a**, **35b** were prepared analogously[27] by reaction of 2-bromo-1-(pyridin-3-yl)-ethanone hydrobromide[30](**59**) and the pertinent phenylthiourea derivatives **58a**, **58b**, which themselves were easily available from 3-nitroaniline (**56a**) and 2-methyl-5-nitroaniline (**56b**) in two steps by a modification of the excellent method described by Rasmussen[31] (Scheme 3).

The substituted carboxylic acids, 4-(2-(*tert*-butoxycarbonylamino)phenylcarbamoyl)benzoic acid (**37**) and 6-(2-(*tert*-butoxycarbonylamino)phenylcarbamoyl)nicotinic acid (**38**) (Scheme 4), which were used for the central amidation step as described in Schemes 1 and 2, were prepared from the corresponding methoxycarbonyl arylic acids **59**, **60** by reaction with *tert*-butyl 2-aminophenylcarbamate[28] (**28**), followed by selective alkaline cleavage of the methyl esters of **61** and **62** with LiOH (Scheme 4).

Following the same strategy for synthesis (Scheme 5), 5-(2-(*tert*-butoxycarbonylamino)phenylcarbamoyl)thiophene-2-carboxylic acid (**39**) was prepared from 5-(methoxycarbonyl)thiophene-2-carboxylic acid[32] (**67**) in two steps. Compound **67** hereby was obtained from thiophene-2-carbaldehyde (**63**) by transformation to 2-(thiophen-2-yl)-1,3-dioxolane[33](**64**), lithiation with *n*-BuLi, introduction of the carboxylic group, and cleavage of the 1,3-dioxolane in one step,[33] followed by esterification of **65**[32] with methyl iodide and oxidation of **66**.

The *N*-hydroxyacrylamide precursors **40** and **41** (Scheme 6) were obtained from the aldehydes **69** and **66** by an aldol condensation with malonic acid in a mixture of pyridine/piperidine,[34] amidation of the resulting acrylic acids **70**,[35]**71** with NH_2OTHP **27**[36] by use of BOP as coupling reagent,[29] and alkaline cleavage of the methyl esters of **72** and **73**, respectively.

Results and Discussion

The in vitro data for inhibition of recombinant HDAC 1 and HDAC 6 (rHDAC1, rHDAC6) as well as inhibition of Abl kinase by chimeric compounds in comparison to **1**, **8**, and **6** as reference compounds are listed in Tables 1−3. In addition to these biochemical data, the cellular efficacy of chimeric HDAC-kinase inhibitors was quantified by induction of cellular histone H3 $K(Ac)^{9+14}$ hyperacetylation and cytotoxicity toward HeLa and K562 cells. Combining the structural features of a 6-methyl-N^1-(4-(pyridin-3-yl)pyrimidin-2-yl)benzene-1,3-diamine (substructure of **1** in Figure 1b) with a *N*-(2-aminophenyl)benzamide or *N*-hydroxyacrylamide motif in general leads to potent rHDAC1 inhibitors, with hydroxamate analogues **10** and **18b** having a potency quite similar to that of **6**. Whereas hydroxamate analogues inhibit rHDAC1 and rHDAC6 as HDAC class I and class II representatives with similar potency, benzamide analogues display weak or no inhibition of rHDAC6. This selectivity, which is illustrated by respective homologues in Tables 2 and 3, was also described for other benzamides.[37,38] For the pyrimidine analogues in Table 2, a minor trend toward more potent inhibition of rHDAC1 and histone H3 hyperacetylation is seen from the pyridine derivative **13b**, to the benzene, **12b**, and thiophene derivative, **14b**.

All rHDAC1 inhibiting compounds induce histone H3 hyperacetlyation in HeLa cells with a potency of EC_{50} around 2 μM, comparable to that of **6** or **8**. Representative concentration-effect curves for histone H3 hyperacetylation in HeLa cells are shown in Figure 2. HeLa cervical carcinoma cells were treated with compounds **12b**, **11**, **10**, **18b**, **16a**, and **14b** for 24 h before fixation and staining with a $H3(K)Ac^{9+14}$ specific antibody and single cell image analysis. EC_{50} values were determined as 1.04 μM (**12b**), 4.8 μM (**11**), 1.5 μM (**10**), 4.2 μM (**18b**), 1.5 μM (**16a**), and 2.6 μM (**14b**).

Different hydroxamate and benzamide derivatives, for example, **10**, **11, 12a/b**, **18a/b**, and **19a/b**, inhibit constitutively active Abl kinase in the biochemical assay with only up to 9-fold lower potency than that of Imatinib. Compound **11** is most active, with an IC_{50} of 2.0 μM. Changing the amine structure to an amide (**12b**), a structural modification that led to the most potent compounds in the parent Imatinib-series,[26] is tolerated but slightly reduces activity in this series. Also, introduction of a heterocycle as a D-ring system (**13b**, **14b**) or use of the *N*-hydroxyacrylamide motif (**10**) decreases Abl kinase inhibition significantly. Most important, the kinase selectivity profile as summarized in Tables 4 and 5 differs from that of **1** with equal inhibition of $AblT^{315}I$ mutant and VEGFR2/KDR. The cytotoxicity of these analogues toward K562 and HeLa CML cell lines toward **1** (K562) or **6** and **8** (K562 and HeLa) is in the low micromolar or sub-micromolar range, corresponding to the range of the IC_{50} values. Nevertheless, the potency of **1** toward K562 cells bearing the Bcr-Abl translocation with $IC_{50} = 0.049$ μM is superior to that of all chimeric compounds.

The benzamide analogues with the bioisosteric (4-((pyridin-3-yl)thiazol-2-ylamino)phenyl)amide substructure (Table 3)

Scheme 2. Synthesis of Target Compounds[a]

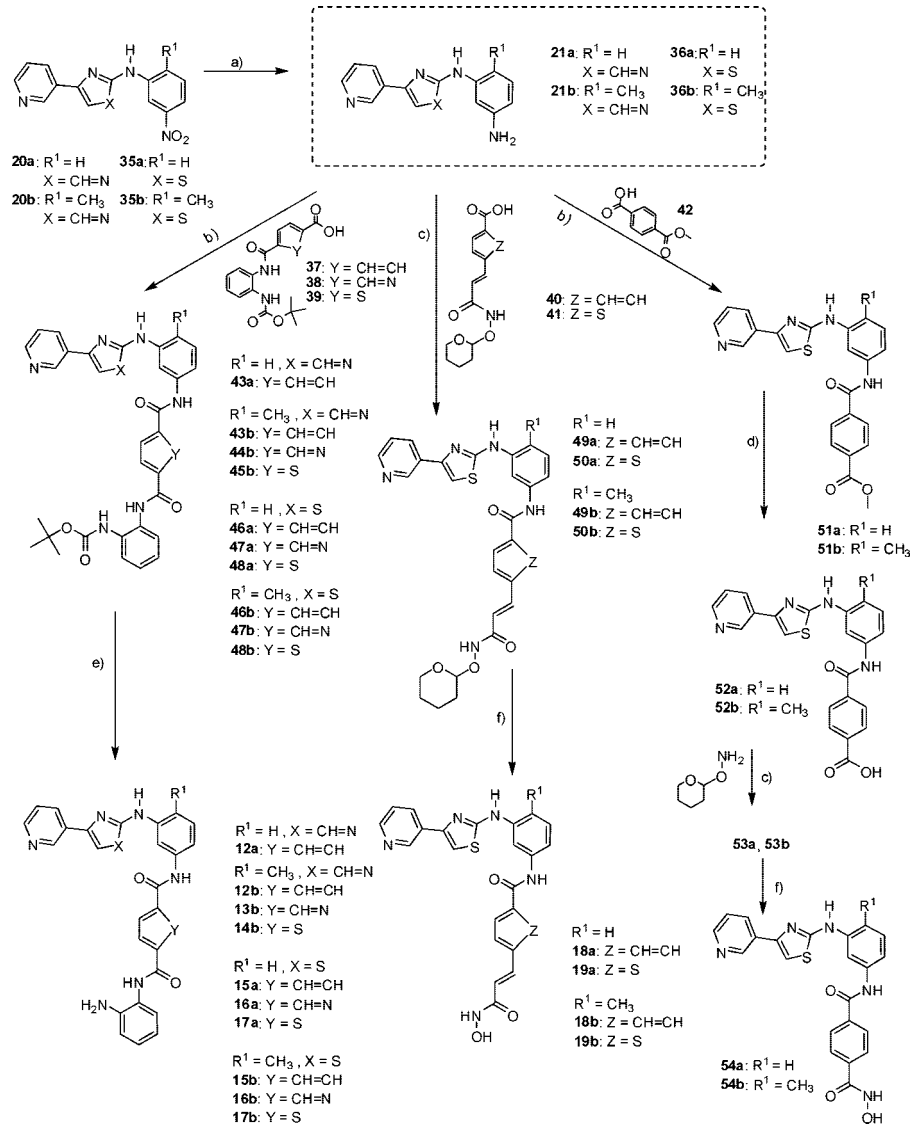

[a] Conditions: (a) H_2, Pd/C, 30 atm, 16 h; (b) $SOCl_2$, pyridine, 20° C; (c) BOP, NEt_3, THF or DMF, 20° C; (d) MeOH, H_2O, LiOH, 20° C, 16 h; (e) CF_3COOH, 20° C, 1 h, then H_2O, NH_3, pH = 9; (f) MeOH, H_2O, HCl, 20° C, 16 h.

Scheme 3[a]

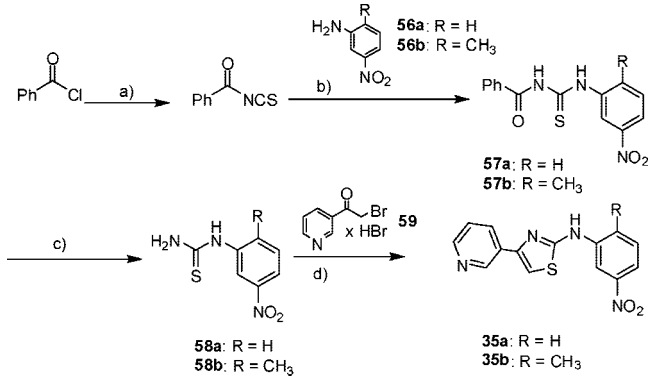

[a] Conditions: (a) NH_4NCS, acetone, Δ, 15 min; (b) acetone, Δ, 30 min, then 0° C, H_2O; (c) LiOH, H_2O, THF, Δ, 6 h; (d) EtOH, Δ, 2 h.

exhibited selective inhibition of rHDAC1 with IC_{50} values in the range of 0.17−1.13 μM. The rHDAC1 inhibitory potency decreases from the benzene derivatives (**15a**, **15b**) to pyridine (**16a**, **16b**) and thiophene derivatives (**17a**, **17b**). Cellular

Scheme 4. Preparation of 4-(2-(*tert*-Butoxycarbonylamino)phenylcarbamoyl)benzoic Acid (**37**) and 6-(2-(*tert*-Butoxycarbonylamino)phenylcarbamoyl)nicotinic Acid (**38**)[a]

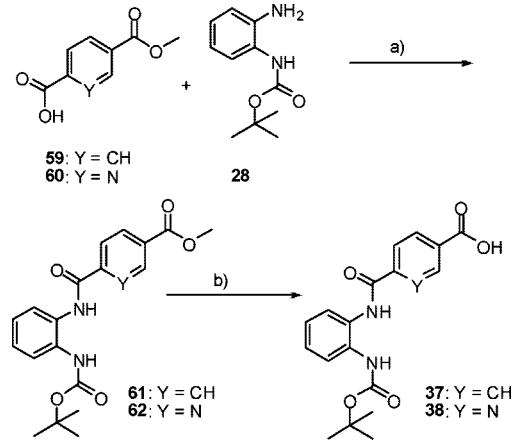

[a] Conditions: (a) BOP, NEt_3, DMF, 20° C; (b) LiOH, MeOH, H_2O, then 0° C, H_2O, HCl, pH = 5.

Scheme 5. Preparation of 5-(2-(*tert*-Butoxycarbonylamino)phenylcarbamoyl)thiophene-2-carboxylic acid (**39**)[a]

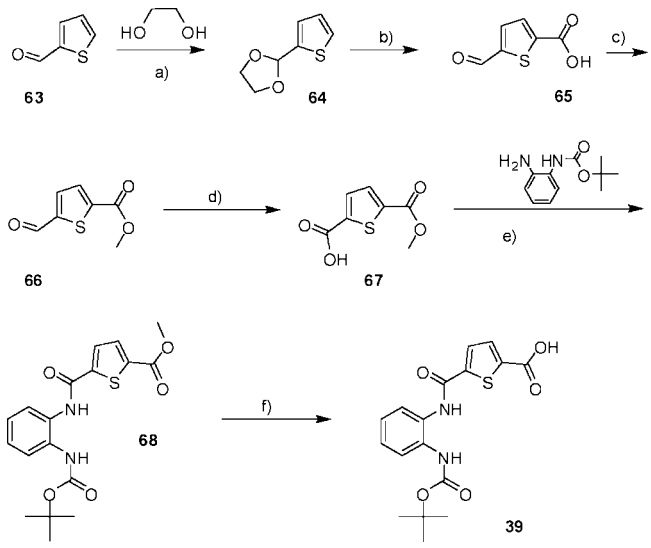

[a] Conditions: (a) Al_2O_3, CCl_4, Δ, 48 h; (b) BuLi, THF, −78° C, then CO_2, followed by H_2SO_4 (10%); (c) CH_3I, Na_2CO_3, DMF, 20° C, 48 h; (d) Jones reagent; (e) BOP, NEt_3, THF, 20° C, 24 h; (f) MeOH, H_2O, LiOH, 24 h.

Scheme 6. Preparation of (*E*)-4-(3-Oxo-3-(tetrahydro-2*H*-pyran-2-yloxyamino)prop-1-enyl)benzoic Acid (**40**) and (*E*)-5-(3-Oxo-3-(tetrahydro-2*H*-pyran-2-yloxyamino)prop-1-enyl)thiophene-2-carboxylic Acid (**41**)[a]

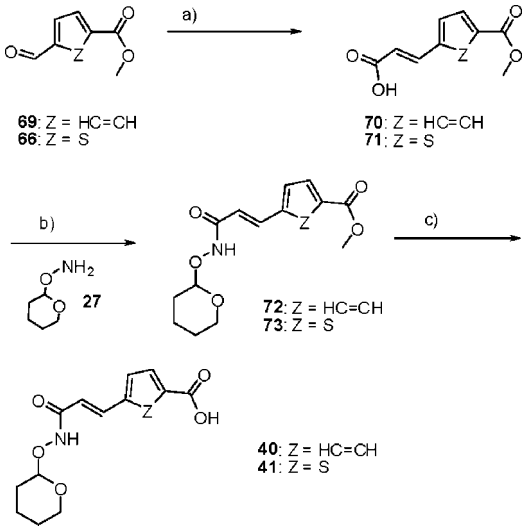

[a] Conditions: (a) $CH_2(COOH)_2$, pyridine, piperidine, 80° C, 3 h; (b) BOP, NEt_3, DMF, 20° C; (c) LiOH, H_2O, MeOH, then 0° C, HCl, pH = 5.

potency as measured by histone H3 hyperacetylation is comparable with EC_{50} values down to 1.15 μM (**15a**). All compounds showed only weak inhibition of Abl kinase. In addition and as seen before, the kinase specificity profile changed compared to that of **1** with a trend toward VEGFR2/KDR inhibition for some analogues (Table 5). Exchange of the benzamide headgroup by the hydroxamate moiety significantly increased rHDAC1 inhibitory activity and led to highly potent inhibition of rHDAC6 (Table 3). These analogues exhibited IC_{50} values for inhibition of rHDAC1 in the range of 0.08−0.21 μM. The "methyl-flag" group at the phenyl C-ring system does not affect rHDAC1 inhibition. Most potent compounds in this series are **18a**, **18b**, and **19b**, bearing the acrylamide motif. Although inhibition of Abl kinase is retained, the selectivity profile is significantly different from that of **1** (Table 5). The cytotoxicity of these thiazolylamino analogues toward HeLa and K562 cells correlates with histone H3 hyperacetylation, with K562 cells being slightly more sensitive (Table 3).

Docking Studies of Compounds 10 and 11 on HDLP and HDAH as well as on Abl and Abl-T^{315}I. Docking studies with the representative compounds **10** and **11** were performed to suggest possible binding modes of the chimeras on HDAC1, HDAC6, Abl, and Abl T^{315}I (Figures 3 and 4). HDAC1 was represented by the crystal structure of a histone deacetylase-like protein (HDLP, PDB code 1c3s[39]) from the hyperthermophilic bacterium *Aquifex aeolicus* sharing 35% identity with human HDAC1 over 375 residues. As a HDAC6 homologue, a histone deacetylase-like amidohydrolase from *Bordetella/Alcaligenes* strain FB188 was used (HDAH, PDB code 1zz1,[40] 35% identity over 291 amino acids with the second domain HDAC6b of human HDAC6). Both structures are in complex with **6**. It was easily possible to dock compound **10** in an energetically favorable conformation into both models. In the minimized complexes, the *N*-hydroxyphenylacrylamide moiety of **10** adopts the same position as the octanedioic acid hydroxyamide chain of **6** (Figure 3A, B). In particular, the interactions with eight amino acids of the active site, conserved in all class I and II HDACs, are similar. The carbonyl and the hydroxy oxygens of the hydroxamic acid are coordinated with the zinc ion. The hydroxy group is hydrogen-bonded with an imidazolyl nitrogen of H^{131} (HDLP) and H^{142} (HDAH), respectively. Another H bond is formed between the carbonyl oxygen and the OH group of Y^{297} (HDLP) or Y^{312} (HDAH). In both models, the phenyl ring is parallelly aligned between two phenylalanine residues (F^{141} and F^{198} in HDLP, F^{152} and F^{208} in HDAH). The 4-((pyridin-3-yl)pyrimidin-2-ylamino)phenyl moiety of **10** projects outward into the solvent (see also Figure 3D), corresponding to the fact that the SARs of the hydroxamates do not strongly depend on variations in this region. Some other amino acids which are conserved between HDLP and HDAC1 or HDAH and HDAC6 lie within a sphere of 3 Å around compound **10**; examples for HDLP are Y^{91} (rHDAC1: E), E^{92} (D), and L^{265} (L), and those for HDAH are L^{21} (mHDAC6: L), D^{98} (D), I^{100} (V), and E^{309} (E).

Compound **11** binds to HDLP in a similar mode as **10**. However, the 2-aminophenylbenzamide moiety must adopt a deeper position in the binding pocket than the hydroxamate group to enable coordination of the carbonyl oxygen with the zinc ion (Figure 3C, D). Two hydrogen bonds of the 2-amino substituent with the backbone of G^{140} and of the carbonyl function with the OH group of Y^{297} may contribute to the tight fit. The phenyl ring of the benzamide moiety is stacked between F^{141}, H^{170}, and F^{198}. Additionally, compound **11** contacts the conserved amino acids M^{130} (rHDAC1: L), C^{142} (C), and L^{265} (L). Just as in the case of the hydroxamate **10**, the 4-((pyridin-3-yl)pyrimidin-2-ylamino)phenyl moiety points outward (Figure 3D). The proposed binding mode of 11 may account for the HDAC1/class I selectivity of the benzamide derivatives. Two significant mutations of glycines strongly narrow the HDAH binding pocket for the 2-aminophenyl group and for the corresponding aryl moieties of the benzamides in Tables 2 and 3, leading to sterical hindrance (Figure 3C). The HDLP residues G^{129} (rHDAC1: G) and G^{294} (G) are mutated in HDAH into P^{140} (mHDAC6: P) and E^{309} (E), respectively. In the aligned crystal structures, the flexible side chain of M^{130} is in place of HDAH P^{140} clashing with compound **11**.

Table 1. Inhibition of rHDAC1, rHDAC6, and c-Abl Kinase, Induction of Histone H3 Hyperacetylation and Cytotoxicity toward HeLa and K562 Cells Mediated by Chimerically Designed 2-Aminophenylpyrimidines as well as **1**, **6**, and **8** as Reference Compounds[a]

example		rHDAC1 inhibition IC_{50} [μM]	rHDAC6 inhibition IC_{50} [μM]	H3K(Ac) induction EC_{50} [μM]	Cytotox HeLa IC_{50} [μM]	Abl inhibiton IC_{50} [μM]	Cytotox K562 IC_{50} [μM]
11	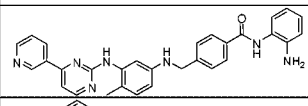	0.208	≥ 32	3.38	1.6)	2.0	0.49
10	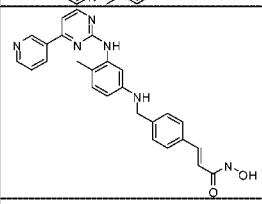	0.077	0.036	1.71	2.65	9.2	0.74
31	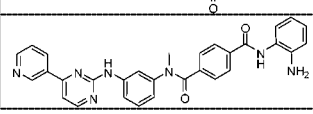	1.16	>100	1.6	9.1	31.0	2.0
1	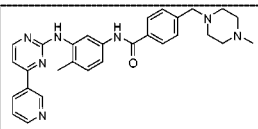	>100	>100	>100	18.65	1.1	0.049
8	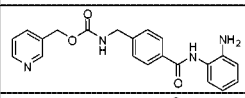	0.74	>100	2.35	3.3	>100	0.72
6	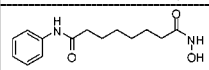	0.02	0.052	6.7	2.2	>100	0.67

[a] Mean IC_{50} values were calculated from respective concentration-effect curves done in replicate using GraphPad Prism statistical analysis software.

Table 2. Inhibition of rHDAC1, rHDAC6, and c-Abl Kinase, Induction of Histone H3 Hyperacetylation and Cytotoxicity toward HeLa and K562 Cells Mediated by Chimerically Designed 2-Aminophenylpyrimidines[a]

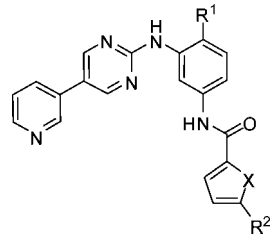

example	R^1	R^2	X	rHDAC1 inhibition IC_{50} [μM]	rHDAC6 inhibition IC_{50} [μM]	H3K(Ac) induction EC_{50} [μM]	Cytotox HeLa IC_{50} [μM]	Abl inhibiton IC_{50} [μM]	Cytotox K562 IC_{50} [μM]
12b	CH_3	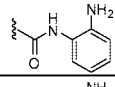	CH=CH	0.27	>100	1.04	1.97	5.3	0.76
13b	CH_3	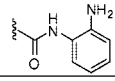	CH=N	0.62	>100	3.9	2.66	32	0.66
14b	CH_3	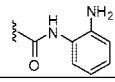	S	0.23	>100	2.6	1.15	25	0.59
12a	H	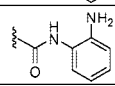	CH=CH	0.76	≥ 32	n.d.	7.13	7.8	1.28

[a] Mean IC_{50} values were calculated from respective concentration-effect curves done in replicate using GraphPad Prism statistical analysis software. (n.d. = not determined).

With respect to Abl and Abl $T^{315}I$, the docking modes of compounds **10** and **11** are rather ambiguous. Based on the crystal structure of Abl in complex with **1** (PDB code 1iep[41]), poses strongly consistent with the binding mode of the cocrystallized

Table 3. Inhibition of rHDAC1, rHDAC6, and c-Abl Kinase, Induction of Histone H3 Hyperacetylation and Cytotoxicity toward HeLa Cells Mediated by Chimerically Designed 2-Aminophenythiazolylamines with a Benazmide or Hydroxamate Head Group[a]

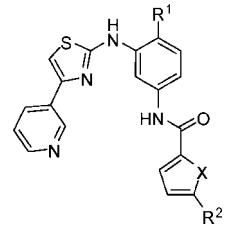

example	R^1	R^2	X	rHDAC1 inhibition IC_{50} [μM]	rHDAC6 inhibition IC_{50} [μM]	H3K(Ac) induction EC_{50} [μM]	Cytotox HeLa IC_{50} [μM]	Abl inhibition IC_{50} [μM]	Cytotox K562 IC_{50}[μM]
Benzamides									
15a	H	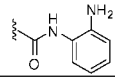	CH=CH	0.23	>32	1.15	3.45	39	0.89
15b	CH_3	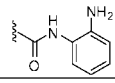	CH=CH	0.17	20.9	1.47	4.45	34	0.85
16a	H	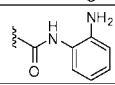	CH=N	0.45	>100	1.7	2.9	24	0.74
16b	CH_3	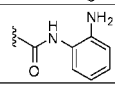	CH=N	0.31	>100	3.0	2.5	35	0.69
17a	H	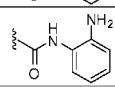	S	0.47	>100	1.74	3.4	24	1.89
17b	CH_3	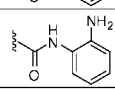	S	1.13	>100	0.46 (20%).	1.28	24	1.15
Hydroxamates									
54a	H	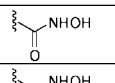	CH=CH	0.21	0.091	7.8	20.3	17	4.45
54b	CH_3	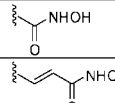	CH=CH	0.17	0.089	4.4	32.6	8.9	3.4
18a	H	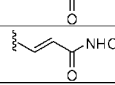	CH=CH	0.10	0.055	1.5	5.92	4.5	1.9
18b	CH_3	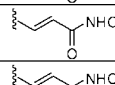	CH=CH	0.08	0.041	4.2	4.64	2.7	0.9
19a	H	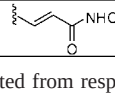	S	0.16	0.045	1.01	8.4	3.8	3.0
19b	CH_3		S	0.12	0.039	2.80	7.3	2.6	2.2

[a] Mean IC_{50} values were calculated from respective concentration-effect curves done in replicate using GraphPad Prism statistical analysis software.

Figure 2. Induction of histone H3 hyperacetylation in HeLa cells.

Table 4. Inhibition of Wild-Type (wt) Abl and Mutant Abl $T^{315}I$, PDGF-Rβ, VEGF-R2/KDR, and PKA by 2-Aminophenylpyrimidines and **1** as Reference[a]

example	Abl (wt) IC_{50} (μM)	ABL $T^{315}I$ IC_{50} (μM)	PDGF-Rβ IC_{50} (μM)	VEGF-R2 IC_{50} (μM)	PKA IC_{50} (μM)
11	2.0	1.12	2.7	7.8	>100
10	9.2	6.9	4.6	9.2	>100
31	31	34	7.3	6.1	38
12b	5.3	4.1	2.6	9.8	>100
13b	32	31	7.8	8.6	>100
14b	25	22	5.2	11	>100
12a	7.8	9.8	1.1	1.5	>100
1	1.1	>100	0.24	25.8	87.5

[a] Mean IC_{50} values were calculated from respective concentration-effect curves done in replicate using GraphPad Prism statistical analysis software.

inhibitor may be suggested (Figure 4A and B). There are exactly the same interactions with Abl if only the corresponding substructures of **1** and **10** are considered. In particular, the hydrogen bonds of the pyridyl nitrogen with the backbone of M^{318} (hinge), of the pyrimidin-2-ylamino group with the side chain of T^{315} (hinge), and of the phenylamino NH with the carboxylate of E^{286} (αC) are reproduced. The *N*-hydroxyacrylamide and the 2-aminophenyl moieties of **10** and **11**, respec-

Table 5. Inhibition of Wild-Type (wt) Abl and Mutant Abl $T^{315}I$, PDGF-Rβ, VEGF-R2/KDR, and PKA[a]

example	Abl (wt) IC_{50} (μM)	ABL $T^{315}I$ IC_{50} (μM)	PDGF-Rβ IC_{50} (μM)	VEGF-R2 IC_{50} (μM)	PKA IC_{50} (μM)
			Benzamides		
15a	39	20	71	24	>100
15b	34	14	8.7	46	>100
16a	24	10	13	4.4	>100
16b	35	12	47	9.0	>100
17a	24	9.0	28	12	>100
17b	24	8.5	11	4.8	>100
			Hxdroxamates		
54a	17	19	40	43	>100
54b	9	8.8	2.1	14	>100
18a	4.5	4	13	8.7	>100
18b	2.7	1.8	3.9	11	>100
19a	3.8	2.0	11	8.6	>100
19b	2.6	1.7	6.2	6.7	>100

[a] Mean IC_{50} values were calculated from respective concentration-effect curves done in replicate using GraphPad Prism statistical analysis software.

tively, are aligned with a mainly hydrophobic pocket between the N- and the C-terminal domain and contact V^{289} (αC), I^{293} (αC), L^{354} (αE), and F^{359} (αE-β7 loop). The *N*-hydroxy group of **10** may form an H bond with the backbone oxygen of I^{360} (αE$-\beta$7 loop). Figure 4B indicates that even longer substituents projecting into the solvent are possible.

However, these "Imatinib modes" do not answer the question why the present compounds are nearly equiactive as inhibitors of Abl and Abl $T^{315}I$, since **1** itself does not bind to the mutant. The problem is complicated by the flexibility of, in particular, the nucleotide binding (P-loop) and the activation loop and thus by the induction of ligand-specific Abl conformations, represented by different crystal structures of the wild-type [PDB code 1m52,[41] complex with 6-(2,6-dichlorophenyl)-8-methyl-2-(3-(methylthio)phenylamino)pyrido[2,3-*d*]pyrimidin-7(8*H*)-one (**74**) (PD173955)][41] and of the Abl $T^{315}I$ mutant [PDB codes 2z60[42] and 2v7a,[43] complexes with (5-[3-(2-methoxyphenyl)-1*H*-pyrrolo[2,3-*b*]pyridin-5-yl]-*N*,*N*-dimethylpyridine-3-carboxamide) (**75**) (PPY-A)[42] and *N*-[5-(2-methoxy-2-phenylacetyl)-1,4,5,6-tetrahydropyrrolo[3,4-*c*]pyrazol-3-yl]-4-(4-methylpiperazin-1-yl)benzamide (**76**) (PHA739358),[44] respectively].

In the "Imatinib mode", the pyrimidinyl ring of **10** is parallelly aligned with F^{382} (DFG motif). This interaction, essential for binding of **1**, requires an inactive, autoinhibiting conformation of the activation loop.[41,45] By contrast, the complex of Abl with **74** represents a conformation of the activation loop like in active kinases.[41] It is impossible to dock compound **10** on this Abl structure in a reasonable conformation. Since the amide analogues **18a** and **18b** (Table 3) are even slightly more potent than **10**, both phenyl rings must be nearly coplanar, which markedly restricts the degrees of conformational freedom. However, compound **10** can be docked into PDB 1m52 (active-like conformation) in an "inverse mode" where the phenylaminomethylphenyl moiety is aligned with the hinge region (Figure 4C). As in the case of the aminopyrimidine group of **74**,[41] an H bond with the backbone oxygen of M^{318} is formed. L^{248} (P-loop) and L^{370} (β7) cover the "inner" phenyl ring from both sides. The *N*-hydroxyacrylamide moiety penetrates into the solvent, which again explains the low variability of the potency within the series. Also corresponding to the SAR, the "methyl-flag" is not involved in direct interactions. The 4-(pyridin-3-yl)pyrimidin-2-ylamino moiety adopts the position of the dichlorophenyl group of **74**, mainly interacting with Y^{253} (P-loop), V^{256} (β2), K^{271} (β3), I^{313} (β5), T^{315} (hinge), D^{381}, and F^{382} (DFG motif). An H bond of the pyridine nitrogen with the protonated amino group of K^{271} is possible.

This "inverse binding mode" of **10** on an active-like Abl wild-type conformation can be almost completely transferred to the structure of the Abl $T^{315}I$ mutant in complex with **75**, also representing an overall active state.[42] Comparing the minimized wild-type and mutant complexes (parts C and D, respectively, of Figure 4), the rms deviation of the Cα atoms amounts to only 1.04 Å. The only significant differences arise from the alignment of the 4-(pyridin-3-yl)pyrimidin-2-ylamino moiety of **10** with the 2-methoxyphenyl group of **75**, leading to interactions, especially with Y^{253} (P-loop), V^{256} (β2), K^{271} (β3), N^{368} (β7), and D^{381} (DFG motif). Again, an H bond of the pyridine nitrogen with the protonated amino group of K^{271} can be suggested.

Since the similar "inverse binding modes" of **10** on active-like conformations of Abl and Abl $T^{315}I$ correspond to the almost equal inhibitory potencies of the present compounds at both Abl species, it could be speculated that indeed active-like states are stabilized in both cases. However, the generation of other ligand-specific conformations not represented by the available crystal structures cannot be ruled out. Therefore, the given binding modes are rather working hypotheses which must be investigated by further experiments.

Selected compounds of all series were pharmacologically characterized in more detail.

The inhibition of PDGF stimulated PDGFRβ autophosphorylation in Swiss 3T3 cells and the constitutive Bcr-Abl phosphorylation in K562 cells were studied, using the benzamide analogues **12b** and **12a** (with and without the "methyl-flag"), the hydroxamate/benzamide homologues **10** and **11,** and the aminothiazolyl hydroxamate derivatives **18b** and **18a** (with and without the "methyl-flag"). As shown in Figure 5, all analogues showed no or only marginal inhibition of cellular Bcr-Abl activity in K562 cells at 1 and 10 μM concentration. This might be explained by a reduced binding to the inactive Bcr-abl protein in cells, in contrast to **1**.

In contrast to the inefficacy of Bcr-abl kinase inhibition in cells, ligand induced PDGFRβ autophosphorylation was potently inhibited by **12b** at 1 and 10 μM, but not by the analog **12a**. A similar result was obtained with **18b** at 10 μM. For both examples, only the analogues with the "methyl-flag" were active cellular PDGFRβ inhibitors. These results are substantiated by a high sensitivity of the eosinophilic leukemia cell line EOL1, bearing the fusion protein FIP1L1-PDGFRα, which causes a constitutive activation of the PDGF-R pathway.[46,47] **12b** and **18b**, in addition to **14b**, are highly cytotoxic toward EOL1 cells with IC_{50} values of 7 and 6 nM, respectively (Table 6). The EOL1 cell line has been described as an in vitro model for chronic eosinophilic leukemia, with idiopathic HES as an indication for Imatinib therapy.[47] Finally, the cytotoxicity profile for the selected compounds of the present series as well as for **1**, **6**, and **8** as reference compounds was evaluated using a panel of 22 to 24 different tumor cell lines emanating from 16 different tumor entities/histotypes.

As summarized in Table 6 and highlighted for **1**, **10**, and **11** (Figure 6), the chimeric compounds are broadly active with a higher potency toward leukemic cell lines K562, EOL1, and CCRF-CEM. The mean inhibitory potency ranges from 3.6 μM for **10** to 7.1 μM for **14b**, quite comparable to that of **6** or **8** with IC_{50} values of 2.6 and 2.8 μM, respectively.

The antiproliferative, cytotoxic activity profiles of **11** and **10** as structural homologues with the benzamide and hydroxamate headgroups in comparison to **1** are shown in Figure 6. The

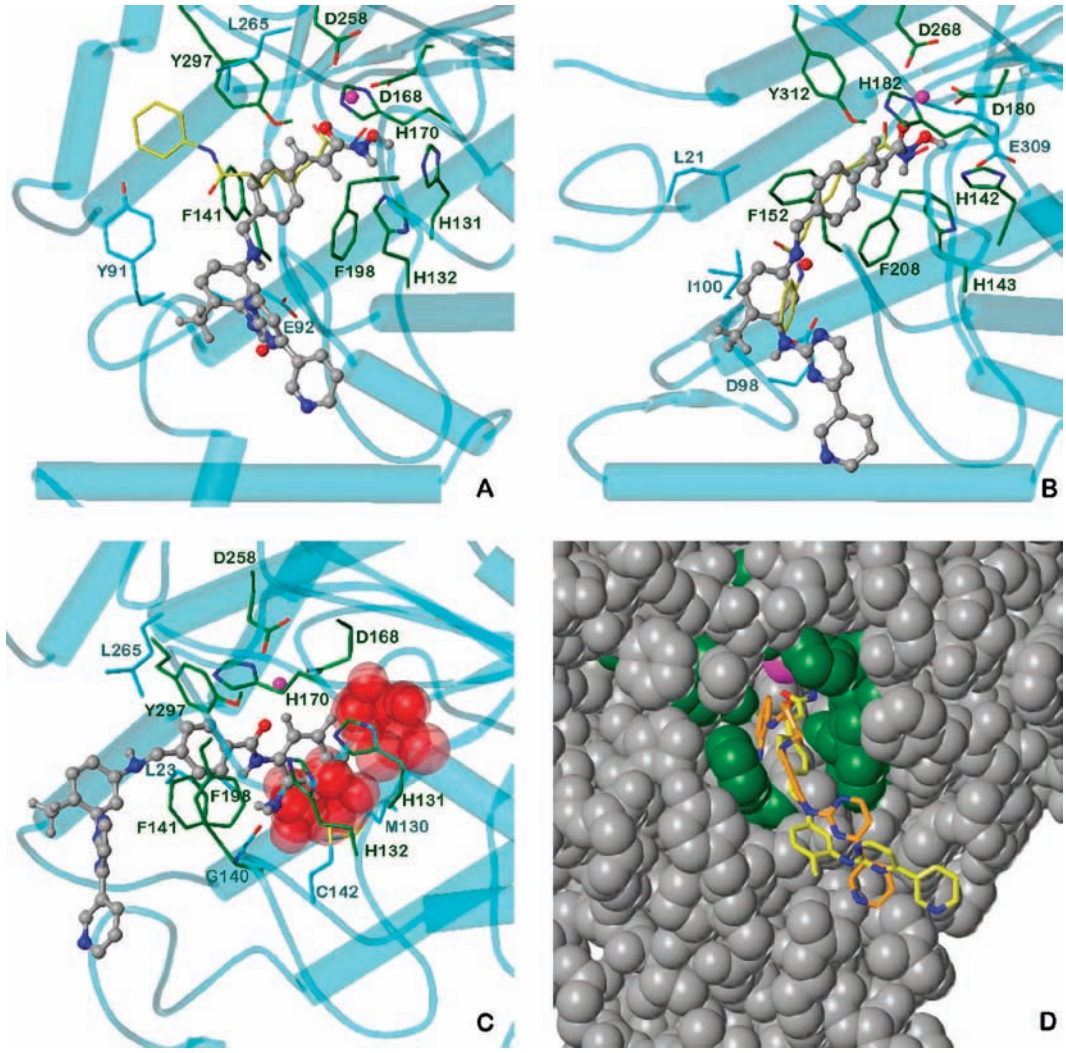

Figure 3. Docking of compounds. **10** and **11** at HDLP (HDAC1 homologue, derived from PDB 1c3s) and HDAH (HDAC6 homologue, derived from PDB 1zz1). Colors of atoms, unless otherwise indicated: O, red; N, blue; S, yellow; Zn^{2+}, magenta. C atoms of the eight conserved amino acids of the binding site, green; C atoms of other residues within a sphere of 3 Å around the ligands, cyan; C and some essential H atoms of **10** and **11**, gray; C atoms of **6**, yellow. The backbones are represented as cyan ribbon (β-sheets) and tube models, and the α-helices are shown as cylinders. (A) Compounds **10** and **6** complexed with HDLP. (B) Compounds **10** and **6** complexed with HDAH. (C) Compound **11** complexed with HDLP. The red CPK models indicate the positions of P^{140} (below) and E^{309} (above) in HDAH (clash with the 2-aminophenyl moiety). (D) CPK model of HDLP with compounds **10** (C atoms yellow) and **11** (C atoms orange) represented as sticks. The eight conserved amino acids of the binding site are green-colored.

deviation from the mean IC_{50} value (shown in parentheses) is given as lgM. For details about the different cell lines and individual IC_{50} values, see the Experimental Part and the Supporting Information, respectively.

Conclusions

In recent studies, combinations of HDIs with the kinase inhibitor **1** showed additive and synergistic effects based on down-regulation of wild-type or mutant Bcr-Abl kinase in blast crisis CML. The chimeric HDAC-kinase inhibitory compounds of the present study are based on the Imatinib scaffold, bearing benzamide or hydroxamate head groups which transfer the HDAC inhibitory property and which determine the selectivity profile, discriminating between hydroxamate-based unselective, pan HDIs and benzamide-based, presumably class I selective HDIs. We could show that the concept of chimeric compounds bearing the pharmacological activities of a HDI as well as a protein kinase inhibitor is feasible. Chimeric compounds based on the structure of **1** with a hydroxamate or benzamide headgroup are potent, broadly active cellular HDAC inhibitors. The HDAC inhibition profile of most chimeras remained conserved in biochemical and cellular assays. Their potency was comparable to that of **6** or **8** as reference HDIs. Inhibition of active Abl kinase in biochemical assays was also conserved in most cases, although inhibition of Bcr-Abl autophosphorylation in K562 CML cells was neclectable and the biochemical selectivity profile was altered. This might be explained by a dimished activity toward the inactive Bcr-abl kinase. Nevertheless, potent cellular inhibition of PDGFR and cytotoxicity toward EOL-1 cells as one feature of **1** is restored in selected analogues, namely **12b**, **14b**, and **18b**. The kinase selectivity profile differed from that of **1** with potent inhibition of the Abl $T^{315}I$ mutant, being resistant to **1**. Docking studies argue in favor of a binding mode "inverse" to that of **1** on an autoinhibiting Abl conformation. Finally, the cytotoxicity toward a broad panel of tumor cell lines emanating from 16 different tumor histotypes was evaluated for selected analogues. In contrast to **1**, all chimeric compounds displayed a broad cytotoxicity with mean IC_{50} values from 3.6 to 7.1 μM, which is comparable to **6**, with a mean IC_{50} of 2.6 μM. Few compounds showed a significantly higher

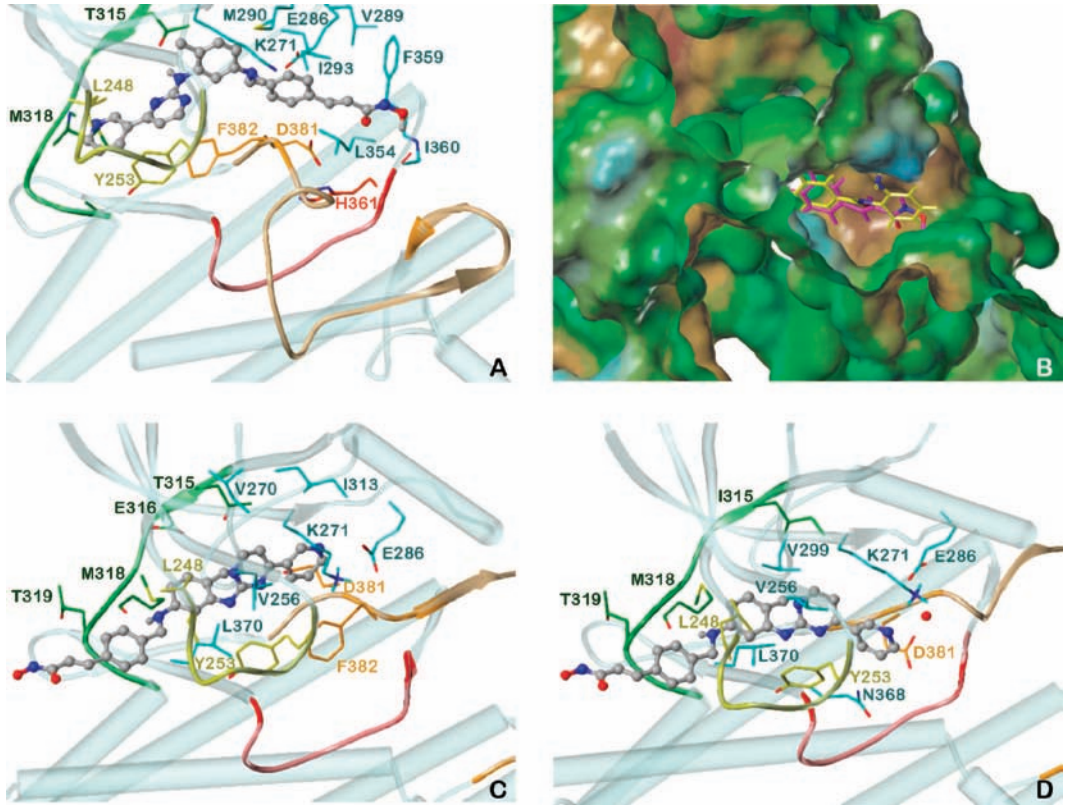

Figure 4. Docking of compounds. **10** and **11** at Abl and Abl-T^{315}I. Colors of atoms, unless otherwise indicated: O, red; N, blue; S, yellow. The Abl backbones are represented as light cyan ribbon (β-sheets) and tube models, and the α-helices are shown as cylinders. Important regions are highlighted: nucleotide binding loop (P-loop), yellow; hinge region, green; catalytic loop, red; activation loop, orange. Drawn are amino acids within a sphere of 3 Å around the ligands. For the C atoms, the same coloring scheme as for the backbone was applied. (A) Compound **10** docked at the Abl structure PDB 1iep (complex with **1**). (B) MOLCAD surface of Abl PDB 1iep (wt abl, inactive conformation) with compounds **10** (C and H atoms magenta) and **11** (C and H atoms yellow). Mapped is the lipophilic potential (color ramp from blue, polar, to brown, hydrophobic). (C) Compound **10** docked on the Abl structure PDB 1m52 (complex with **74**). (D) Compound **10** docked on the Abl-T^{315}I structure PDB 2z60 (complex with **75**).

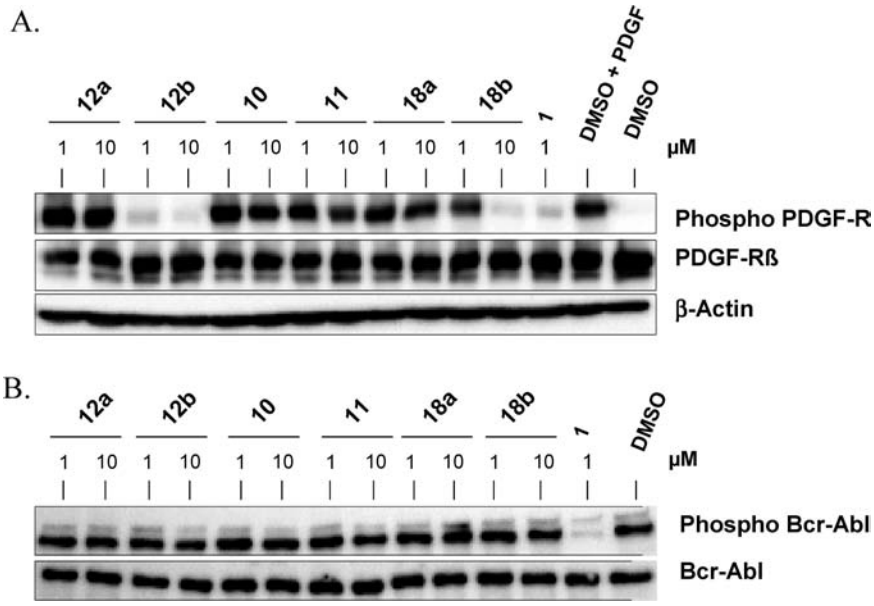

Figure 5. Analysis of Bcr-Abl and PDGFRβ phosphophorylation in K562 and Swiss 3T3 cells. K562 CML (A) and PDGF stimulated Swiss 3T3 cells (B) were treated with chimeric compounds at 1 and 10 μM concentration, as indicated for 1−3 h before cell lysis and Western blot analysis, detecting c-abl phosphoY^{245}, c-Abl, and phosphorylated PDGFRβ proteins. As a loading control, membranes were reprobed with an antibody specific for β-Actin. Cells treated with 1 μM of **1** or 0.5 vol % DMSO were included as a positive and negative control, respectively.

activity toward the EOL1 chronic eosinophilic leukemia cell line, a model for HES treated clinically with **1**. This correlated with the potent inhibition of ligand activated PDGFR in 3T3 fibroblast cells by chimeric compounds **12b** and **18b**. Thus, these

Table 6. Anti-proliferative, Cytotoxic Activity of Selected Compounds Evaluated Using a Panel of 22 to 25 Different Human Tumor Cell Lines (Number of Individual Tumor Cell Lines in Parenthesis)[a]

example	mean cytotox IC_{50} (μM)	cytotox CCRF-CEM IC_{50} (μM)	cytotox K562 IC_{50} (μM)	cytotox EOL-1 IC_{50} (μM)	cytotox A549 IC_{50} (μM)
6	2.6 (22)	0.8	0.67	1.0	2.2
8	2.8 (22)	0.71	0.72	0.053	3.3
1	27.6 (25)	36	0.049	0.0002	15.5
12b (B)	5.2 (24)	2.0	0.76	0.007	3.57
14b (B)	7.1 (25)	1.4	0.59	0.003	2.61
10 (H)	3.6 (24)	0.73	0.74	0.11	3.42
11 (B)	6.1 (24)	2.0	0.49	0.10	2.60
16a (B)	4.7 (25)	1.8	0.74	0.12	3.74
18b (H)	5.2 (25)	1.3	0.9	0.006	6.62

[a] Mean IC_{50} values are given in the first column with the sensitivity of selected cell lines CCRF-CEM (ALL), K562 (CML), EOL1 (HES), and A549 (NSCLC) shown for comparison. For details regarding cell lines, see the Experimental Part. (B, benzamide analog; H, hyxdroxamate analog.) Cytotoxicity on selected cell lines is shown by mean IC_{50} values, calculated from respective concentration-effect curves done in replicate using GraphPad Prism statistical analysis software.

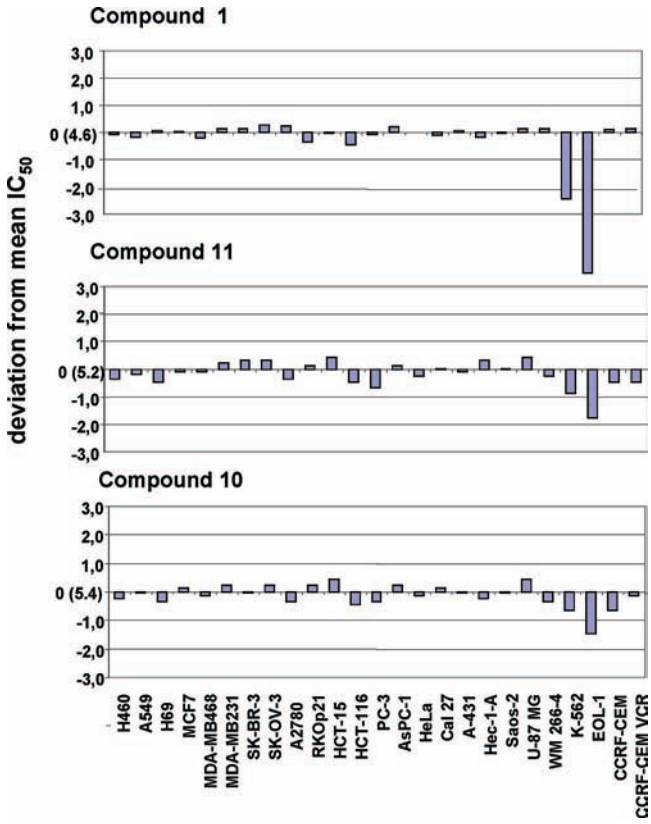

Figure 6. Cytotoxicity profile of selected compounds.

analogues most likely bear one feature of **1**, conferring selective cytotoxicity toward PDGFR driven diseases such as HES. We conclude that chimeric HDAC-kinase inhibitory compounds are a new approach for the combination therapy of cancer.

Experimental Section

Biological Methods. Biochemical HDAC Assays. For rHDAC1 and rHDAC6 expression, a clonal HEK293 (ATCC CRL1573) human kidney cell line expressing the human rHDAC1 isoenzyme bearing a C-terminal flag epitope was provided by E. Verdin, The Gladstone Institute/San Francisco, CA. The rHDAC1 and rHDAC6 proteins were purified by M2-affinity gel chromatography according to the manufacturer's protocol (Sigma #A2220). Purified protein

Chart 1. Chemical Structures of **74**, **75**, and **76**

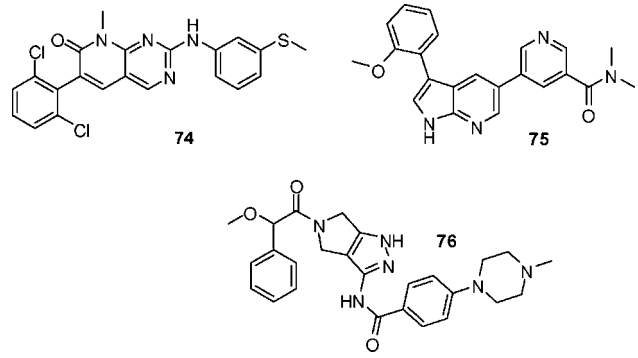

samples were routinely analyzed by SDS-PAGE (12.5% or 10% Laemmli gels) followed by Coomassie stain and Western blotting using a FLAG-specific antibody (anti M2-POX antibody, Sigma #A8592) followed by ECL-detection (GE Healthcare). In addition, protein batches were analyzed by Western blotting for various HDAC isoenzymes including HDAC1 and HDAC6.

The biochemical HDAC activity assay was essentially done as described by Wegener et al.[48]

For further details, see the Supporting Information.

Biochemical Protein Kinase Assays. Active kinase proteins were either obtained from commercial suppliers (Abl, PDGF-Rβ ProQinase, Freiburg/Germany; AblT^{315}I: Millipore/Upstate, Billerica/USA; protein kinase A (PKA): InvitroGen/Panvera, Carlsbad/USA) or prepared in-house (KDR, c-terminal kinase domain AA790-1356). As substrates, poly-AGKY for Abl, AblT^{315}I, and PDGF-Rβ (#P-1152 Sigma, Munich/Germany), poly-GT for KDR (#P-0275, Sigma, Munich/Germany) or a PKA substrate peptide for PKA (#12-394, Millipore/Upstate, Billerica/USA) were used. Into each well of a 96-well flashplate (#SMP-200 in the case of Abl, AblT^{315}I, PDGF-Rβ, and KDR, #SMP-103 in the case of PKA; Perkin-Elmer, Waltham/USA) kinase protein was diluted into kinase assay buffer (50 mM HEPES pH 7.5, 3 mM $MgCl_2$, 3 mM $MnCl_2$, 1 mM DTT, 3 μM sodium orthovanadate, 5 μg/mL PEG 8000) containing the appropriate substrate (final volume 89 μL). DMSO vehicle or compounds are added as 1 μL/well prior to the initiation of the kinase reaction by 10 μL 1 mM [^{33}P]-γATP (4×10^5 cpm). Reactions were allowed to proceed for a time predetermined to show a linear dependence on a time versus phosphorylation plot (30 min for PKA, otherwise 80 min) and terminated with the addition of an equal volume of phosphoric acid (2% H_3PO_4 for 5 min). Plates were washed three times with 0.9% w/v NaCl and quantitated by liquid scintillation counting.

Cellular Histone H3 Hyperacetylation Assay. To assess the cellular efficacy of a histone deacetylase inhibition, an assay was set up for use on the Cellomics "ArrayScan II" platform for a quantitative calculation of histone acetylation as described.[49]

Cellular Proliferation Assay. The antiproliferative activity of selected compounds was evaluated using numerous tumor cell lines.[37,50] For quantification of cellular proliferation/cytotoxicity, the Alamar Blue (Resazurin) cell viability assay was applied.[51] For further details, see the Supporting Information.

Western Blot Analysis. For Western blot analysis, 1.9×10^6/well K562 or 1×10^6/well NIH 3T3 cells in six well cell culture plates were treated with the test compounds for 3 or 2 h, respectively. Next, NIH3T3 cells were stimulated with 50 ng/mL of human recombinant PDGF-BB for 10 min at room temperature before cell lysis. Cells were lysed in 200 or 300 μL lysis buffer (50 mM Tris HCl pH 8, 150 mM NaCl, 1v/v NP-40, 0.5% w/v sodium desoxycholate, 0.2% w/v sodiumdodecylsulfate (SDS), 0.02% w/v NaN_3, 1 mM sodium vanadate, 20 mM NaF, 100 μg/mL PMSF, 10 mM sodiumpyrophosphate, protease inhibitor mix/Roche and 50 U/ml Benzonase) at 4 °C. Respective equal amounts of protein were separated by SDS-PAGE before transfer to polyvinylidendifluoride (PVDF) membrane (Biorad Art. No. 162-0177) by semidry blotting. The following antibodies were used:

monoclonal mouse antibody specific for β-Actin (clone AC-12, Sigma Art. No. A-5441), polyclonal rabbit antibody specific for c-abl kinase (Cell Signaling #2862), polyclonal rabbit antibody specific for phospho c-abl Y^{245} (Cell Signaling #2861), polyclonal rabbit antibody specific for PDGF-Rβ (Santa Cruz #sc-432), mouse monoclonal antibody clone 4G10 specific for posphotyrosine (Upstate #05-321), goat antirabbit IgG-HRP conjugated (Biorad: 170-6515), and goat-antimouse IgG-HRP conjugated (Biorad: 170-6516).

Chemical Procedures

General. NMR spectra were recorded with a Bruker Avance 300 MHz spectrometer at 300 K, using TMS as an internal standard. IR spectra (KBr or pure solid) were measured with a Bruker Tensor 27 spectrometer. Melting points were determined with a Büchi B-545. MS spectra were measured with a Finnigan MAT 95 (EI, 70 eV) or with a Finnigan Thermo Quest TSQ 7000 (ESI) (DCM/MeOH + 10 mmol/L NH_4Ac), respectively. All reactions were carried out under nitrogen. Elemental analyses were performed by the Analytical Laboratory of the University of Regensburg. Chemical names were created using ChemDraw Ultra 10.0 software.

***N*-(2-Methyl-5-nitrophenyl)-4-(pyridin-3-yl)pyrimidin-2-amine (20b)** was prepared as described.[27]

6-Methyl-N^1-(4-(pyridin-3-yl)pyrimidin-2-yl)benzene-1,3-diamine (21b).[26] ^{1}H NMR (DMSO-d_6): δ (ppm) = 2.09 (s, 3 H), 4.85 (bs, 2 H), 6.35 (dd, 1 H, J = 2.4 Hz, J = 8.1 Hz), 6.80 (m, 2 H), 7.35 (m, 1 H), 7.51 (dd, 1 H, J = 5.0 Hz, J = 8.0 Hz), 8.46 (m, 1 H), 8.69 (m, 2 H), 9.24 (d, 1 H, J = 2.4 Hz).

Preparation of (*E*)-3-(4-(Methoxycarbonyl)phenyl)acrylic Acid (70) and (*E*)-3-(5-(Methoxycarbonyl)thiophen-2-yl)acrylic Acid (71). A mixture of the respective aldehyde (**69** or **66**, 15.0 mmol), malonic acid (30.0 mmol), and pyridine/piperidine (2:1; 3.75 mL) was heated to 80 °C for 3 h. The hot mixture was poured into water (20 mL) under stirring and acidified with diluted HCl. The mixture was cooled in an ice bath, and the precipitating crystals were removed by filtration, washed with diluted HCl, and dried in vacuo.

(*E*)-3-(4-(Methoxycarbonyl)phenyl)acrylic Acid (70).[35] ^{1}H NMR (DMSO-d_6): δ (ppm) = 3.87 (s, 3H), 6.66 (d, 1H, J = 16.0 Hz), 7.64 (d, 1H, J = 16.1 Hz), 7.83 (d, 2H, J = 8.3 Hz), 7.97 (d, 2H, J = 8.3 Hz), 12.57 (s, 1H).

Preparation of Carboxylic Acid Methyl Esters (61, 62, 68, 72, and 73) by Amidation with 28 or NH_2OTHP (*O*-(Tetrahydro-2*H*-pyran-2-yl)hydroxylamine) (27). The respective methoxycarbonyl aroylic acid (10.0 mmol) (**59**, **60**, **70**, **71**, or **52a** and **52b**) was dissolved in dry THF (50.0 mL) or DMF (20.0 mL), and 1.1 equiv of BOP (benzotriazolyloxy-tris-(dimethylamino)phosphoniumhexafluorophosphate), 2.2 equiv of NEt_3, and 1.1 equiv of the respective amine (**28**[28] or NH_2OTHP **27**[36]) were added. After stirring at room temperature for 24 h, the mixture was poured into water with stirring, and the precipitating product was filtered off, dried in vacuo, and purified by column chromatography (CH_2Cl_2/MeOH = 10/1).

Methyl 4-(2-(*tert*-Butoxycarbonylamino)phenylcarbamoyl)benzoate (61).[52] ^{1}H NMR (DMSO-d_6): δ (ppm) = 1.44 (s, 9H), 3.91 (s, 3H), 7.22 (dt, 1H, J = 1.8 Hz, J = 7.7 Hz), 7.15 (dt, 1H, J = 1.7 Hz, J = 7.6 Hz), 7.55 (m, 2H), 8.10 (m, 4H), 8.71 (s, 1H), 9.98 (s, 1H).

(*E*)-Methyl 4-(3-Oxo-3-(tetrahydro-2*H*-pyran-2-yloxyamino)-prop-1-enyl)benzoate (72). ^{1}H NMR (DMSO-d_6): δ (ppm) = 1.54 (s, 3H), 1.70 (s, 3H), 3.54 (dd, 1H, J = 4.6 Hz, J = 6.9 Hz), 3.86 (s, 3H), 4.02 (m, 1H), 4.93 (s, 1H), 6.63 (d, 1H, J = 15.9 Hz), 7.55 (d, 1H, J = 15.8 Hz), 7.72 (d, 2H, J = 8.2 Hz), 7.98 (d, 2H, J = 8.3 Hz), 11.34 (s, 1H). Anal. ($C_{16}H_{19}NO_5$) C, H, N.

Preparation of Suitably Protected and Substituted Carboxylic Acids 37, 38, 39, 40, and 41 by Alkaline Cleavage of the Corresponding Carboxylic Acid Methyl Esters. The respective methyl esters **61**, **62**, **68**, **72**, and **73** (5.0 mmol) were dissolved in MeOH (50 mL), and 2 equiv of LiOH in H_2O (50 mL) was added. After stirring at room temperature overnight, MeOH was removed under reduced pressure, and the aqueous layer was extracted with ethyl acetate (3 × 20 mL), cooled to 0 °C, and acidified with diluted acetic acid to pH = 5−6. The precipitating product was removed by filtration and dried in vacuo.

4-(2-(*tert*-Butoxycarbonylamino)phenylcarbamoyl)benzoic Acid (37).[53] ^{1}H NMR (DMSO-d_6): δ (ppm) = 1.44 (s, 9H), 7.15 (dt, 1H, J = 1.6 Hz, J = 7.6 Hz), 7.22 (dt, 1H, J = 1.8 Hz, J = 7.7 Hz), 7.55 (dt, 2H, J = 1.5 Hz, J = 7.8 Hz), 8.07 (m, 4H), 8.73 (s, 1H), 9.97 (s, 1H), 13.33 (s, 1H).

5-(2-(*tert*-Butoxycarbonylamino)phenylcarbamoyl)thiophene-2-carboxylic Acid (39).[54] ^{1}H NMR (DMSO-d_6): δ (ppm) = 1.45 (s, 9H), 7.16 (m, 2H), 7.26 (d, 1H, J = 3.8 Hz), 7.51 (m, 2H), 7.77 (d, 1H, J = 3.8 Hz), 8.75 (s, 1H), 9.87 (s, 1H).

(*E*)-4-(3-Oxo-3-(tetrahydro-2*H*-pyran-2-yloxyamino)prop-1-enyl)benzoic Acid (40). ^{1}H NMR (DMSO-d_6): δ (ppm) = 1.54 (s, 3H), 1.70 (s, 3H), 3.54 (dd, 1H, J = 4.6 Hz, J = 6.9 Hz), 3.98 (m, 1H), 4.93 (s, 1H), 6.62 (d, 1H, J = 15.8 Hz), 7.54 (d, 1H, J = 15.7 Hz), 7.69 (d, 2H, J = 8.1 Hz), 7.96 (d, 2H, J = 8.3 Hz), 11.34 (s, 1H). Anal. ($C_{15}H_{17}NO_5 \cdot {}^3/_2H_2O$) C, H, N.

***tert*-Butyl 2-(4-(4-Methyl-3-(4-(pyridin-3-yl) pyrimidin-2-ylamino) phenylcarbamoyl) benzamido)phenylcarbamate (43b).** 4-(2-(*tert*-Butoxycarbonylamino)phenylcarbamoyl)benzoic acid (**37**)[53] (0.68 g, 1.91 mmol) was dissolved in dry THF (20.0 mL) and BOP (benzotriazolyloxy-tris-(dimethylamino)phosphoniumhexafluorophosphate) (2.00 mmol, 0.88 g), and NEt_3 (0.60 mL, 4.19 mmol) and 6-methyl-N^1-(4-(pyridin-3-yl)pyrimidin-2-yl)benzene-1,3-diamine (**21b**)[26] (0.50 g, 1.91 mmol) were added. After stirring at room temperature for 24 h, the mixture was poured into water with stirring, and the precipitating product was filtered off, dried in vacuo, and purified by column chromatography (CH_2Cl_2/MeOH = 8/1).

^{1}H NMR (DMSO-d_6): δ (ppm) = 1.45 (s, 9H), 2.25 (s, 3H), 7.22 (m, 3H), 7.43 (d, 1H, J = 5.6 Hz), 7.53 (m, 4H), 8.11 (m, 5H), 8.49 (m, 2H), 8.68 (m, 2H), 8.96 (s, 1H, exchangeable), 9.28 (s, 1H), 9.95 (s, 1H, exchangeable), 10.40 (s, 1H, exchangeable). Anal. ($C_{35}H_{33}N_7O_4 \cdot {}^1/_2H_2O$) C, H, N.

Preparation of Carbamic Acid *tert*-Butyl Esters 44b, 45b, 46a, 46b, 47a, 47b, 48a, and 48b by Amidation of the Respective Carboxylic Acids. The respective carboxylic acid was dissolved in 10 mL of dry pyridine, and 1.1 equiv of $SOCl_2$ was added. The mixture was stirred at room temperature for half an hour, and 1.0 equiv of the respective arylamine was added. After stirring at room temperature for 24 h, the mixture was poured into water with stirring, and the precipitating product was removed by filtration, dried in vacuo, and purified by column chromatography (DCM/MeOH = 10/1).

***tert*-Butyl-2-(5-(4-methyl-3-(4-(pyridin-3-yl)pyrimidin-2-ylamino)phenylcarbamoyl)picolinamido)phenylcarbamate (44b).** ^{1}H NMR (DMSO-d_6): δ (ppm) = 1.51 (s, 9H), 2.26 (s, 3H), 7.19 (m, 1H), 7.28 (m, 3H), 7.46 (d, 1H, J = 5.2 Hz), 7.53 (m, 2H), 8.02 (d, 1H, J = 8.1 Hz), 8.13 (d, 1H, J = 1.9 Hz), 8.32 (d, 1H, J = 8.2 Hz), 8.50 (m, 1H), 8.54 (d, 1H, J = 5.2 Hz), 8.58 (dd, 1H, J = 2.1 Hz, J = 8.2 Hz), 8.70 (dd, 1H, J = 1.5 Hz, J = 4.7 Hz), 9.03 (s, 1H), 9.12 (d, 1H, J = 1.6 Hz), 9.18 (s, 1H), 9.30 (d, 1H, J = 1.8 Hz), 10.57 (s, 1H), 10.62 (s, 1H). Anal. ($C_{34}H_{32}N_8O_4 \cdot {}^1/_2H_2O$) C, H, N.

***tert*-Butyl 2-(5-(4-Methyl-3-(4-(pyridin-3-yl)pyrimidin-2-ylamino)phenylcarbamoyl)thiophene-2-carboxamido)phenylcarbamate (45b).** ^{1}H NMR (DMSO-d_6): δ (ppm) = 1.46 (s, 9H), 2.24 (s, 3H), 7.15 (dt, 1H, J = 1.6 Hz, J = 7.6 Hz), 7.23 (m, 2H), 7.46 (m, 1H), 7.50 (dd, 2H, J = 1.2 Hz, J = 7.8 Hz), 7.55 (m, 2H), 7.94 (d, 1H, J = 4.0 Hz), 8.07 (m, 2H), 8.50 (m, 1H), 8.53 (d, 1H, J = 5.2 Hz), 8.70 (dd, 1H, J = 1.6 Hz, J = 4.8 Hz), 8.77 (s, 1H), 9.01 (s, 1H), 9.29 (d, 1H, J = 1.7 Hz), 9.97 (s, 1H), 10.38 (s, 1H). Anal. ($C_{33}H_{31}N_7O_4S \cdot {}^3/_4H_2O$) C, H, N.

Preparation of 12b, 13b, 14b, 15a, 16a, 17a, 15b, 16b, and 17b by Cleavage of the *tert*-Butyl Phenylcarbamate Group. General procedure: The respective carbamic acid *tert*-butyl-esters **30**, **44b**, **45b**, **46a**, **46b**, **47a**, **47b**, **48a**, and **48b** were dissolved in TFA (5.0 mL for 0.5 mmol ester) and stirred at room temperature for 2 h. The solution was poured into water (100 mL) under stirring, and the mixture was alkalized with NH_3 (pH = 9). The precipitating product was filtered off, washed with H_2O, and dried in vacuo.

***N*^{1}-(2-Aminophenyl)-*N*^{4}-(4-methyl-3-(4-(pyridin-3-yl)pyrimidin-2-ylamino)phenyl)terephthalamide (12b).** ^{1}H NMR (DMSO-d_6): δ (ppm) = 2.24 (s, 3H), 4.95 (s, 2H), 6.58−6.64 (m, 1H), 6.80 (dd, 1H, J = 8.0 Hz, J = 1.1 Hz), 6.96−7.02 (m, 1H), 7.19 (d, 1H, J = 7.7 Hz), 7.23 (d, 1H, J = 8.2 Hz), 7.44 (d, 1H, J = 5.2 Hz), 7.50−7.55 (m, 2H), 8.06−8.15 (m, 5H), 8.47−8.51 (m, 1H), 8.52 (d, 1H, J = 5.2 Hz), 8.69 (dd, 1H, J = 4.8 Hz, J = 1.5 Hz), 8.99 (s, 1H), 9.28 (d, 1H, J = 1.6 Hz), 9.91 (s, 1H), 10.36 (s, 1H). Anal. ($C_{30}H_{25}N_7O_2 \cdot {}^1/_2H_2O$) C, H, N.

***N*^{2}-(2-Aminophenyl)-*N*^{5}-(4-methyl-3-(4-(pyridin-3-yl)pyrimidin-2-ylamino)phenyl)thiophene-2,5-dicarboxamide (14b).** ^{1}H NMR (DMSO-d_6): δ (ppm) = 2.24 (s, 3H), 6.63 (dt, 1H, J = 1.0 Hz, J = 7.7 Hz), 6.81 (dd, 1H, J = 1.0 Hz, J = 8.0 Hz), 7.01 (dt, 1H, J = 1.3 Hz, J = 8.0 Hz), 7.15 (dd, 1H, J = 1.0 Hz, J = 7.7 Hz), 7.24 (d, 1H, J = 8.4 Hz), 7.46 (m, 2H), 7.54 (dd, 1H, J = 4.8 Hz, J = 7.9 Hz), 8.02 (m, 2H), 8.08 (d, 1H, J = 1.8 Hz), 8.52 (m, 2H), 8.70 (dd, 1H, J = 1.4 Hz, J = 4.7 Hz), 9.01 (s, 1H), 9.29 (d, 1H, J = 1.7 Hz), 9.88 (s, 1H), 10.35 (s, 1H). Anal. ($C_{28}H_{23}N_7O_2S$) C, H, N.

Preparation of *N*-(Tetrahydro-2*H*-pyran-2-yloxy)amides 49a, 49b and 50a, 50b by Amidation of the Respective Carboxylic Acids 40 and 41. The respective carboxylic acid was dissolved in the necessary amount of dry DMF, and 1.1 equiv of BOP, 2.0 equiv of NEt_3, and 1.1 equiv of the respective arylamine were added. After stirring at room temperature for 24 h, the mixture was poured into water under stirring, and the precipitating product was removed by filtration, dried *in vacuo*, and purified by column chromatography (DCM/MeOH = 10/1).

(*E*)-*N*-(4-Methyl-3-(4-(pyridin-3-yl)thiazol-2-ylamino)phenyl)-4-(3-oxo-3-(tetrahydro-2*H*-pyran-2-yloxyamino)prop-1-enyl)benzamide (49b). ^{1}H NMR (DMSO-d_6): δ (ppm) = 1.55 (s, 3H), 1.71 (s, 3H), 2.28 (s, 3H), 3.55 (m, 1H), 3.97 (m, 1H), 4.94 (s, 1H), 6.64 (d, 1H, J = 15.9 Hz), 7.20 (d, 1H, J = 8.5 Hz), 7.38 (dd, 1H, J = 2.1 Hz, J = 8.2 Hz), 7.43 (ddd, 1H, J = 0.6 Hz, J = 4.9 Hz, J = 8.0 Hz), 7.49 (s, 1H), 7.57 (d, 1H, J = 15.9 Hz), 7.75 (d, 2H, J = 8.2 Hz), 8.01 (d, 2H, J = 8.4 Hz), 8.33 (m, 1H), 8.49 (dd, 1H, J = 1.6 Hz, J = 4.7 Hz), 8.66 (d, 1H, J = 2.0 Hz), 9.17 (d, 1H, J = 1.7 Hz), 9.48 (s, 1H), 10.30 (s, 1H), 11.33 (s, 1H). Anal. ($C_{30}H_{29}N_5O_4S \cdot {}^1/_2H_2O$) C, H, N.

Preparation of *N*-Hydroxyamides 10, 18a, 18b, 19a, 19b, and 54a, 54b by Cleavage of the Respective *N*-(Tetrahydro-2*H*-pyran-2-yloxy)amides (49a, 49b, 50a, 50b, and 53a, 53b). The respective *N*-(tetrahydro-2*H*-pyran-2-yloxy)amide was dissolved in the necessary amount of MeOH, 1 N HCl (half of the amount of MeOH) was added, and the mixture was stirred at room temperature overnight. The organic solvent was removed *in vacuo*, and the product was filtered off, washed with a small amount of MeOH, and dried in vacuo.

(*E*)-4-(3-(Hydroxyamino)-3-oxoprop-1-enyl)-*N*-(4-methyl-3-(4-(pyridin-3-yl)thiazol-2-ylamino)phenyl)benzamide Hydrochloride Hydrate (18b). ^{1}H NMR (DMSO-d_6): δ (ppm) = 2.29 (s, 3H), 6.64 (d, 1H, J = 15.9 Hz), 7.20 (d, 1H, J = 8.4 Hz), 7.34 (dd, 1H, J = 2.0 Hz, J = 8.2 Hz), 7.54 (d, 1H, J = 15.8 Hz), 7.73 (d, 2H, J = 8.3 Hz), 7.89 (s, 2H), 8.08 (m, 4H), 8.80 (dd, 1H, J = 0.9 Hz, J = 5.7 Hz), 8.95 (d, 1H, J = 1.9 Hz), 9.09 (m, 1H), 9.46 (d, 1H, J = 1.7 Hz), 9.67 (s, 1H), 10.36 (s, 1H), 10.96 (s, 1H). Anal. ($C_{25}H_{21}N_5O_3S \cdot {}^3/_2H_2O \cdot HCl$) C, H, N.

Molecular Modeling. Docking studies were performed with the molecular modeling package SYBYL 7.3 (Tripos L. P., St. Louis, MO) on a Silicon Graphics Octane workstation. The following crystal structures from the Brookhaven Protein Databank were used as raw models for the docking of compounds **10** and/or **11**: HDLP-SAHA[39] (PDB code 1c3s), HDAH-SAHA[40] (1zz1), Abl-Imatinib[41] (1iep), Abl-PD173955[41] (1m52), and AblT^{315}I-PPY-A[42] (1z60). Hydrogens were added, and AMBER_FF99 charges were assigned to the proteins and the water molecules. In HDLP and HDAH, the Zn ions received formal charges of 2. The cocrystallized ligands served as templates for initial conformations and for the manual docking of **10** and **11**, directed by optimal overlap of corresponding substructures and taking into account torsional flexibility closely around local energy minima. The inhibitors were provided with Gasteiger−Hueckel charges. Each complex was refined in a stepwise approach. First, minimization (100 cycles of steepest descent, then Powell conjugate gradient) with fixed ligand (AMBER_FF99 force field,[55] dielectric constant of 4) until a root-mean-square (rms) force of 0.1 kcal mol^{-1} Å^{-1} was approached, second, minimization of the ligand and the surrounding (distance up to 6 Å) protein residues (Tripos force field,[56] dielectric constant of 1, Powell), and, third, again minimization with fixed ligand (AMBER_FF99 force field, dielectric constant of 4, Powell). The second and the third steps were stopped at an rms force of 0.05 kcal mol^{-1} Å^{-1}. Molecular surfaces and lipophilic potentials (protein variant with the new Crippen parameter table[57,58]) were calculated and visualized by the program MOLCAD (J. Brickmann et al., Technical University of Darmstadt, Germany) contained within SYBYL.

Acknowledgment. We thank E. Verdin, Gladstone Institute for Virology and Immunology, San Francisco, CA, for providing rHDAC1 and rHDAC6 expressing Hek293 cell lines. We also thank colleagues at ALTANA−Nycomed Discovery Research, in particular U. Bosch and G. Quintini, for providing rHDAC and kinase protein preparations as well as C. Burkhardt, H. Wieland, C. Engesser, and H. Julius for excellent technical assistance.

Supporting Information Available: Full experimental details for synthetic preparations, analytical data of all compounds, and biological test systems are available free of charge via the Internet at http://pubs.acs.org.

References

(1) Dancey, J.; Sausville, E. A. Issues and progress with protein kinase inhibitors for cancer treatment. *Nat. Rev. Drug Discovery* **2003**, *2*, 296–313.

(2) Shah, N. P.; Nicoll, J. M.; Nagar, B.; Gorre, M. E.; Paquette, R. L.; Kuriyan, J.; Sawyers, C. L. Multiple BCR-ABL kinase domain mutations confer polyclonal resistance to the tyrosine kinase inhibitor imatinib (STI571) in chronic phase and blast crisis chronic myeloid leukemia. *Cancer Cell* **2002**, *2*, 117–125.

(3) Daub, H.; Specht, K.; Ullrich, A. Strategies to overcome resistance to targeted protein kinase inhibitors. *Nat. Rev. Drug. Discovery* **2004**, *3*, 1001–10.

(4) Talpaz, M.; Shah, N. P.; Kantarjian, H.; Donato, N.; Nicoll, J.; Paquette, R.; Cortes, J.; O'Brien, S.; Nicaise, C.; Bleickardt, E.; Blackwood-Chirchir, M. A.; Iyer, V.; Chen, T. T.; Huang, F.; Decillis, A. P.; Sawyers, C. L. Dasatinib in imatinib-resistant Philadelphia chromosome-positive leukemias. *N. Engl. J. Med.* **2006**, *354*, 2531–2541.

(5) Branford, S.; Rudzki, Z.; Walsh, S.; Grigg, A.; Arthur, C.; Taylor, K.; Herrmann, R.; Lynch, K. P.; Hughes, T. P. High frequency of point mutations clustered within the adenosine triphosphate-binding region of BCR/ABL in patients with chronic myeloid leukemia or Ph-positive acute lymphoblastic leukemia who develop imatinib (STI571) resistance. *Blood* **2002**, *99*, 3472–3475.

(6) Weisberg, E.; Griffin, J. D. Mechanism of resistance to the ABL tyrosine kinase inhibitor STI571 in BCR/ABL-transformed hematopoietic cell lines. *Blood* **2000**, *95*, 3498–3505.

(7) Weisberg, E.; Griffin, J. D. Mechanisms of resistance imatinib (STI571) preclinical models and in leukemia patients. *Drug Resistance Updates* **2001**, *4*, 22–28.

(8) le Coutre, P.; Tassi, E.; Varella-Garcia, M.; Barni, R.; Mologni, L.; Cabrita, G.; Marchesi, E.; Supino, R.; Gambacorti-Passerini, C. Induction of resistance to the Abelson inhibitor STI571 in human leukemic cells through gene amplification. *Blood* **2000**, *95*, 1758–1766.

(9) Mahon, F. X.; Deininger, M. V.; Schultheis, B.; Reiffers, J.; Goldman, J. M.; Melo, J. V. Selection and characterization of BCR-ABL-positive cell lines with differential sensitivity to the tyrosine kinase inhibitor STI 571: diverse mechanisms of resistance. *Blood* **2000**, *96*, 1070–1079.

(10) Lombardo, L. J.; Lee, F. Y.; Chen, P.; Norris, D.; Barrish, J. C.; Behnia, K.; Castaneda, S.; Cornelius, L. A.; Das, J.; Doweyko, A. M.; Fairchild, C.; Hunt, J. T.; Inigo, I.; Johnston, K.; Kamath, A.; Kan, D.; Klei, H.; Marathe, P.; Pang, S.; Peterson, R.; Pitt, S.; Schieven, G. L.; Schmidt, R. J.; Tokarski, J.; Wen, M. L.; Wityak, J.; Borzilleri, R. M. Discovery of *N*-(2-chloro-6-methyl-phenyl)-2-(6-(4-(2-hydroxyethyl)-piperazin-1-yl)-2-methylpyrimidin-4- ylamino)thiazole-5-carboxamide (BMS-

354825), a dual Src/Abl kinase inhibitor with potent antitumor activity in preclinical assays. *J. Med. Chem.* **2004**, *47*, 6658–6661.

(11) Weisberg, E.; Manley, P. W.; Breitenstein, W.; Brueggen, J.; Cowan-Jacob, S.; Sandra, W.; Ray, A.; Huntly, B.; Fabbro, D.; Fendrich, G.; Hall-Meyers, E.; Kung, A. L.; Mestan, J.; Daley, G. Q.; Callahan, L.; Catley, L.; Cavazza, C.; Azam, M.; Neuberg, D.; Wright, R. D.; Gilliland, D. G.; Griffin, J. D. Characterization of AMN107, a selective inhibitor of native and mutant Bcr-Abl. *Cancer Cell* **2005**, *7*, 129–141.

(12) Kantarjian, H.; Giles, F.; Wunderle, L.; Bhalla, K.; O'Brien, S.; Wassmann, B.; Tanaka, C.; Manley, P.; Rae, P.; Mietlowski, W.; Bochinski, K.; Hochhaus, A.; Griffin, J. D.; Hoelzer, D.; Albitar, M.; Dugan, M.; Cortes, J.; Alland, L.; Ottmann, O. G. Nilotinib in imatinib-resistant CML and Philadelphia chromosome-positive ALL. *N. Engl. J. Med.* **2006**, *354*, 2542–2551.

(13) Nimmanapalli, R.; Fuino, L.; Bali, P.; Gasparetto, M.; Glozak, M.; Tao, J.; Moscinski, L.; Smith, C.; Wu, J.; Jove, R.; Atadja, P.; Bhalla, K. Histone Deacetylase Inhibitor LAQ824 Both Lowers Expression and Promotes Proteasomal Degradation of Bcr- Abl and Induces Apoptosis of Imatinib Mesylate-sensitive or -refractory Chronic Myelogenous Leukemia-Blast Crisis Cells. *Cancer Res.* **2003**, *63*, 5126–5135.

(14) George, P.; Bali, P.; Annavarapu, S.; Scuto, A.; Fiskus, W.; Guo, F.; Sigua, C.; Sondarva, G.; Moscinski, L.; Atadja, P.; Bhalla, K. Combination of the histone deacetylase inhibitor LBH589 and the hsp90 inhibitor 17-AAG is highly active against human CML-BC cells and AML cells with activating mutation of FLT-3. *Blood* **2005**, *105*, 1768–1776.

(15) Yu, C.; Rahmani, M.; Almenara, J.; Subler, M.; Krystal, G.; Conrad, D.; Varticovski, L.; Dent, P.; Grant, S. Histone deacetylase inhibitors promote STI571-mediated apoptosis in STI571-sensitive and -resistant Bcr/Abl+ human myeloid leukemia cells. *Cancer Res.* **2003**, *63*, 2118–2126.

(16) Fiskus, W.; Pranpat, M.; Balasis, M.; Bali, P.; Estrella, V.; Kumaraswamy, S.; Rao, R.; Rocha, K.; Herger, B.; Lee, F.; Richon, V.; Bhalla, K. Cotreatment with vorinostat (suberoylanilide hydroxamic acid) enhances activity of dasatinib (BMS-354825) against imatinib mesylate-sensitive or imatinib mesylate-resistant chronic myelogenous leukemia cells. *Clin. Cancer Res.* **2006**, *12*, 5869–5878.

(17) Remiszewski, S. W.; Sambucetti, L. C.; Bair, K. W.; Bontempo, J.; Cesarz, D.; Chandramouli, N.; Chen, R.; Cheung, M.; Cornell-Kennon, S.; Dean, K.; Diamantidis, G.; France, D.; Green, M. A.; Howell, K. L.; Kashi, R.; Kwon, P.; Lassota, P.; Martin, M. S.; Mou, Y.; Perez, L. B.; Sharma, S.; Smith, T.; Sorensen, E.; Taplin, F.; Trogani, N.; Versace, R.; Walker, H.; Weltchek-Engler, S.; Wood, A.; Wu, A.; Atadja, P. N-hydroxy-3-phenyl-2-propenamides as novel inhibitors of human histone deacetylase with in vivo antitumor activity: discovery of (2*E*)-*N*-hydroxy-3-[4-[[(2-hydroxyethyl)[2-(1*H*-indol-3-yl)ethyl]amino]methyl]phenyl]-2-propenamide (NVP-LAQ824). *J. Med. Chem.* **2003**, *46*, 4609–4624.

(18) Kelly, W. K.; O'Connor, O. A.; Krug, L. M.; Chiao, J. H.; Heaney, M.; Curley, T.; MacGregore-Cortelli, B.; Tong, W.; Secrist, J. P.; Schwartz, L.; Richardson, S.; Chu, E.; Olgac, S.; Marks, P. A.; Scher, H.; Richon, V. M. Phase I study of an oral histone deacetylase inhibitor, suberoylanilide hydroxamic acid, in patients with advanced cancer. *J. Clin. Oncol.* **2005**, *23*, 3923–3931.

(19) de Ruijter, A. J. M.; van Gennip, A. H.; Caron, H. N.; Kemp, S.; van Kuilenburg, A. B. P. Histone deacetylases (HDACs): characterization of the classical HDAC family. *J. Biochem.* **2003**, *370*, 737–749.

(20) Minucci, S.; Pelicci, P. G. Histone deacetylase inhibitors and the promise of epigenetic (and more) treatments for cancer. *Nat. Rev. Cancer* **2006**, *6*, 38–51.

(21) Johnstone, R. W.; Licht, J. D. Histone deacetylase inhibitors in cancer therapy: is transcription the primary target. *Cancer Cell* **2003**, *4*, 13–18.

(22) Sasakawa, Y.; Naoe, Y.; Sogo, N.; Inoue, T.; Sasakawa, T.; Matsuo, M.; Manda, T.; Mutoh, S. Marker genes to predict sensitivity to FK228, a histone deacetylase inhibitor. *Biochem. Pharmacol.* **2005**, *69*, 603–616.

(23) Garber, K. HDAC inhibitors overcome first hurdle. *Nat. Biotechnol.* **2007**, *25*, 17–19.

(24) Dokmanovic, M.; Clarke, C.; Marks, P. A. Histone Deacetylase Inhibitors: Overview and Perspectives. *Mol. Cancer. Res.* **2007**, *5*, 981–989.

(25) Zimmermann, J.; Buchdunger, E.; Mett, H.; Meyer, T.; Lydon, N. B.; Traxler, P. (Phenylamino)pyrimidine (PAP)-Derivatives: A new class of potent and highly selective PDGFR Autophosphorylation Inhibitors. *Bioorg. Med. Chem. Lett.* **1996**, *6*, 1221–1226.

(26) Zimmermann, J.; Buchdunger, E.; Mett, H.; Meyer, T.; Lydon, N. B. Potent and selective inhibitors of the ABL-kinase: phenylaminopyrimidine (PAP) derivatives. *Bioorg. Med. Chem. Lett.* **1997**, *7*, 187–192.

(27) Szakacs, Z.; Beni, S.; Varga, Z.; Oerfi, L.; Keri, G.; Noszal, B. Acid-Base Profiling of Imatinib (Gleevec) and Its Fragments. *J. Med. Chem.* **2005**, *48*, 249–255 .

(28) Petasis, N. A.; Patel, Z. D. Synthesis of piperazinones and benzopiperazinones from 1,2-diamines and organoboronic acids. *Tertrahedron Lett.* **2000**, *41*, 9607–9611.

(29) Castro, B.; Dormoy, J. R.; Evin, G.; Selve, C. Peptide coupling reagents. IV. N-[Oxytris(dimethylamino)phosphonium]benzotriazole hexafluorophosphate. *Tetrahedron Lett.* **1975**, *14*, 1219–1222.

(30) Callahan, J. F.; Burgess, J. L.; Fornwald, J. A.; Gaster, L. M.; Harling, J. D.; Harrington, F. P.; Heer, J.; Kwon, C.; Lehr, R.; Mathur, A.; Olson, B. A.; Weinstock, J.; Laping, N. J. Identification of Novel Inhibitors of the Transforming Growth Factor β 1 (TGF-β 1) Type 1 Receptor (ALK5). *J. Med. Chem.* **2002**, *45*, 999–1001.

(31) Rasmussen, C. R.; Villani, F. J.; Weaner, L. E.; Reynolds, B. E.; Hood, A. R.; Hecker, L. R.; Nortey, S. O.; Hanslin, A.; Costanzo, M. J.; Powell, E. T.; Molinari, A. J. Improved Procedures for the Preparation of Cycloalkyl-, Arylalkyl-, and Arylthioureas. *Synthesis* **1988**, *6*, 456–459.

(32) Goddard, C. J. 5-Heteroaryl-2-thiophenecarboxylic acids: oxazoles and oxadiazoles. *J. Heterocycl. Chem.* **1991**, *28*, 17–28.

(33) Carpenter, A. J.; Chadwick, D. J. Chemoselective protection of heteroaromatic aldehydes as imidazolidine derivatives. Preparation of 5-substituted furan- and thiophene-2-carboxaldehydes via metallo-imidazolidine intermediates. *Tetrahedron* **1985**, *41*, 3803–3812.

(34) Kluger, R.; Shen, L.; Xiao, H.; Jones, R. T. Systematically Cross-Linked Human Hemoglobin: Functional Effects of 10.ANG. Spans between Beta Subunits at Lysine-82. *J. Am. Chem. Soc.* **1996**, *118*, 8782–8786.

(35) Nagao, Y.; Inoue, K.; Yamaki, M.; Takagi, S.; Fujita, E. New aldose reductase inhibitors. Part I. Syntheses of (rac)3-substituted 4-methoxycarbonyl-1,3-thiazolidine-2-thiones via rearrangement of a substituted group from exo-S to N in (rac)2-substituted thio-4-methoxycarbonyl-Δ 2−1,3-thiazolines. *Chem. Pharm. Bull.* **1988**, *36*, 495–508.

(36) Martin, N. I.; Woodward, J. J.; Marletta, M. A. NG-Hydroxyguanidines from Primary Amines. *Org. Lett.* **2006**, *8*, 4035–4038.

(37) Beckers, T.; Burkhardt, C.; Wieland, H.; Gimmnich, P.; Ciossek, T.; Maier, T.; Sanders, K. Distinct pharmacological properties of 2nd generation HDAC inhibitors with the benzamide or hydroxamate head group. *Int. J. Cancer* **2007**, *121*, 1138–1148.

(38) Kalita, A.; Bonfils, C.; Maroun, C.; Fournel, M.; Rahil, G.; Yan, T. P.; Lu, A.; Reid, G. K.; Besterman, J. M.; Zuomei, L. Pharmacodynamic assessment of MGCD0103, a novel isotype-specific HDAC inhibitor, in preclinical evaluations and phase I trials. AACR-NCI-EORTC conference, Philadelphia, PA, 2005, Abstract C216.

(39) Finnin, M. S.; Donigian, J. R.; Cohen, A.; Richon, V. M.; Rifkind, R. A.; Marks, P. A.; Breslow, R.; Pavletich, N. P. Structures of a histone deacetylase homologue bound to the TSA and SAHA inhibitors. *Nature* **1999**, *401*, 188–193.

(40) Nielsen, T. K.; Hildmann, C.; Dickmanns, A.; Schwienhorst, A.; Ficner, R. Crystal structure of a bacterial class 2 histone deacetylase homologue. *J. Mol. Biol.* **2005**, *354*, 107–120.

(41) Nagar, B.; Bornmann, W. G.; Pellicana, P.; Schindler, T.; Veach, D. R.; Miller, W. T.; Clarkson, B.; Kuriyan, J. Crytal structure of the kinase domain of c-Abl in complex with the small molecule inhibitors PD173955 and imatinib (STI-571). *Cancer Res.* **2002**, *62*, 4236–4243.

(42) Zhou, T.; Parillon, L.; Li, F.; Wang, Y.; Keats, J.; Lamore, S.; Xu, Q.; Shakespeare, W.; Dalgarno, D.; Zhu, X. Crystal structure of the T315I mutant of Abl kinase. *Chem. Biol. Drug Des.* **2007**, *70*, 171–181.

(43) Modugno, M.; Casale, E.; Soncini, C.; Rosettani, P.; Colombo, R.; Lupi, R.; Rusconi, L.; Fancelli, D.; Carpinelli, P.; Cameron, A. D.; Isacchi, A.; Moll, J. Crystal structure of the T315I Abl mutant in complex with the aurora kinases inhibitor PHA-739358. *Cancer Res.* **2007**, *67*, 7987–90.

(44) Carpinelli, P.; Ceruti, R.; Giorgini, M. L.; Cappella, P.; Gianellini, L.; Croci, V.; Degrassi, A.; Texido, G.; Rocchetti, M.; Vianello, P.; Rusconi, L.; Storici, P.; Zugnoni, P.; Arrigoni, C.; Soncini, C.; Alli, C.; Patton, V.; Marsiglio, A.; Ballinari, D.; Pesenti, E.; Fancelli, D.; Moll, J. PHA-739358, a potent inhibitor of Aurora kinases with a selective target inhibition profile relevant to cancer. *Mol. Cancer Ther.* **2007**, *6*, 3158–3168.

(45) Schindler, T.; Bornmann, W.; Pellicena, P.; Miller, W. T.; Clarkson, B.; Kuriyan, J. Structural mechanism for STI-571 inhibition of abelson tyrosine kinase. *Science* **2000**, *289*, 1938–42.

(46) Griffin, J. H.; Leung, J.; Bruner, R. J.; Caligiuri, M. A.; Briesewitz, R. Discovery of a fusion kinase in EOL-1 cells and idiopathic hypereosinophilic syndrome. *Proc. Natl. Acad. Sci.* **2003**, *100*, 7830–7835.

(47) Cools, J.; Quentmeier, H.; Huntly, B. J.; Marynen, P.; Griffin, J. D.; Drexler, H. G.; Gilliland, D. G. The EOL-1 cell line as an in vitro model for the study of FIP1L1-PDGFRA-positive chronic eosinophilic leukemia. *Blood* **2004**, *103*, 2802–2805.

(48) Wegener, D.; Wirsching, F.; Riester, D.; Schwienhorst, A. A fluorogenic histone deacetylase assay well suited for high-throughput activity screening. *Chem. Biol.* **2003**, *10*, 61–68.

(49) Braunger, J.; Zoche, M.; Schmidt; Wiesbacher, M.; Burkhardt, C.; Gekeler, V.; Beckers, T. High content profiling of HDAC inhibitors in cellular assays. AACR Annual Conference, 2003, Abstract 4556.

(50) Dehmel, F.; Weinbrenner, S.; Julius, H.; Ciossek, T.; Maier, T.; Stengel, T.; Fettis, K.; Burkhardt, C.; Wieland, H.; Beckers, T. Trithiocarbonates as a novel class of HDAC inhibitors: SAR studies, isoenzyme selectivity, and pharmacological profiles. *J. Med. Chem.* **2008**, *51*, 3985–4001.

(51) O'Brian, J.; Wilson, I.; Orton, T.; Pognan, F. Investigation of the Alamar Blue (resazurin) fluorescent dye for the assessment of mammalian cell toxicity. *Eur. J. Biochem.* **2000**, *267*, 5421–5426.

(52) Delorme, D.; Woo, S. H.; Vaisburg, A.; Moradei, O.; Leit, S.; Raeppel, S.; Frechette, S.; Bouchain, G. Preparation of triazinyl and other carboxamides as inhibitors of histone deacetylase. US 2005288282 A1, 2005.

(53) Schuppan, D.; Herold, C.; Gansmayer, M.; Ocker, M.; Thierauch, K.-H. Preparation of N-aryl benzamides as histone deacetylase inhibitors. PCT Int. Appl. WO 2004058234 A2, 2004.

(54) Fertig, G.; Herting, F.; Kubbies, M.; Limberg, A.; Reiff, U.; Weidner, M. Preparation of new mono-acylated o-phenylendiamines derivatives as HDAC inhibitors for treating cancer. PCT Int. Appl. WO 2004069803, 2004.

(55) Cornell, W. D.; Cieplak, P.; Bayly, C. I.; Gould, I. R.; Merz, K. M. J.; Ferguson, D. M.; Spellmeyer, D. C.; Fox, T.; Caldwell, J. W.; Kollman, P. A. A second generation force field for the simulation of proteins and nucleic acids. *J. Am. Chem. Soc.* **1995**, *117*, 5179–5197.

(56) Clark, M.; Cramer, R. D. I.; Van Opdenbosch, N. Validation of the general purpose tripos 5.2 force field. *J. Comput. Chem.* **1989**, *10*, 982–1012.

(57) Ghose, A. K.; Viswanadhan, V. N.; Wendoloski, J. J. Prediction of Hydrophobic (Lipophilic) Properties of Small Organic Molecules Using Fragmental Methods: An Analysis of ALOGP and CLOGP Methods. *J. Phys. Chem.* **1998**, *102*, 3762–3772.

(58) Heiden, W.; Moeckel, G.; Brickmann, J. A new approach to analysis and display of local lipophilicity/hydrophilicity mapped on molecular surfaces. *J. Comput. Aided Mol. Des.* **1993**, *7*, 503–14.

JM800988R